DESIGN OF STRUCTURES FOR PROTECTION FROM WINDOW-COLLIMATED, CEILING-SCATTERED FALLOUT RADIATION

763

by

ROBERTO IOTTI

B.S., Kansas State University, 1964

A MASTER'S THESIS

submitted in partial fulfillment of the
requirements for the degree

MASTER OF SCIENCE

Department of Nuclear Engineering

KANSAS STATE UNIVERSITY

Manhattan, Kansas

1967

Approved by:

Richard E. Faw

Major Professors

TABLE OF CONTENTS

LIST OF TABLES

LIST OF FIGURES

NOMENCLATURE

a	Dose angular distribution empirical constant
a'	Build-up factor constant
$\underline{a}$	Dose rate albedo defined by Eq. (24)
A	Least squares constant
a_c	Gaussian quadrature weights defined for the x integration
a_j	Gaussian quadrature weights defined for the θ integration
a_k	Gaussian quadrature weights defined for the ϕ integration
a_m	Gaussian quadrature weights defined for the y integration
A_{1-5}	Constants in Chilton-Huddleston formula
b	Build-up factor constant
b'	Parameter defined in Eq. (96)
B	Dose build-up factor for isotropic source defined by Eq. (10)
B'	Least squares constant
c	Velocity of light
c'	Parameter defined in Eq. (96)
C,C'	Chilton-Huddleston constants
d	Distance between ceiling of i^{th} floor in multistory building and source plane (feet)
d'	Distance between ceiling and floor, feet (Figure 2)
dA	Elemental area in an infinite plane isotropic source
D	Displacement of the window center from the x = 0 position, feet
D'	Dose rate registered by an isotropic detector at a height d above an infinite plane source of radiation
D_i	Total incident dose rate at a point (x,y) in the ceiling
D_o	Dose rate at a height of 3 feet above an infinitely contaminated plane, (reference dose rate)

D_r	Differential reflected dose rate at a point (x,y) in the ceiling
D_u	Dose rate from unscattered radiation at a distance r from a point isotropic source
$\bar{D}$	Dose rate at a point (xx,yy,zz)
e	Charge of the electron
E	Energy of radiation reflected from the ceiling
E_o	Energy of incident radiation
F	Total flux from a point isotropic source defined by Eq. (14)
F_a	Parameter defined by Eq. (25)
F_{pli}	Dose angular distribution of radiation for a plane isotropic source, not normalized
F_u	Unscattered flux from a point isotropic source defined by Eq. (13)
h	Sill height (feet)
H	Distance from the ceiling to the horizontal centerline of the aperture, feet (Figure 2)
K	Order of Gaussian quadrature in integrations over polar and azimuthal angles
l	Dose angular distribution of radiation from an infinite plane isotropic source integrated over all azimuthal angles
l'	Dose angular distribution of radiation from an infinite plane isotropic source of radiation normalized to D_o
L	Order of Gaussian quadrature employed in x-integration
l_u	Dose angular distribution of unscattered radiation from an infinitely contaminated plane, normalized to D_o
m	Mass of the electron
m'	Parameter defined in Eq. (96)
M	Order of Gaussian quadrature employed in y-integration
N_{pli}	Differential photon flux from a plane isotropic source of radiation
p	Ratio of emergent to incident energy
P	Percentage aperture

r	Distance from point isotropic source to detector
r'	Radial distance in plane surface geometry, feet (Figure 5)
R	Aperture half-width, feet
R_E	Eccentricity correction factor defined in Figure 9
R_F	Reduction factor for first floors of square buildings defined in Figure 7
R.F.	Reduction factor at a point (xx,yy,zz)
R_s	Sill height correction factor defined in Figure 10
R_u	Upper stories correction factor defined in Figure 11
R_x	Secondary eccentricity correction factor defined in Figure 10a
R_0	Variable distance between contaminated plane and position (x,y) on ceiling, feet (Figure 5)
R_0'	Classical radius of the electron
t	Thickness of floors, feet
u_i	Zeroes of the Legendre polynomials for the order of Gaussian quadrature employed
V	Aperture half-height, feet
w_i	Christoffel numbers defined for the Gaussian quadrature
W	Constant of proportionality defined by Eq. (11)
x	Ceiling rectangular coordinate parallel to plane of aperture, feet
x_f	Distance from a point to a plane source of radiation measured in psf.
XMAX	Half-width of the ceiling, feet
xx	Detector rectangular coordinate parallel to plane of aperture, feet
y	Ceiling rectangular coordinate perpendicular to plane of aperture, feet
$\tilde{y}$	Dummy variable in y-integration
YMAX	Total length of the ceiling, feet
yy	Detector rectangular coordinate perpendicular to plane of aperture, feet

zz	Perpendicular distance measured positive downward from the ceiling, feet

Greek Symbols

α	Conversion factor defined by Eq. (5)
ε	Eccentricity defined in Eq. (49)
η	Parameter defined in Eq. (49)
θ	Polar angle of reflection, radians
θ_0	Polar angle of incidence, radians
θ_1, θ_2	Polar limits of the aperture, radians
θ_s	Total scattering angle defined by Eq. (21), radians
κ	Ratio of Compton scattering energies multiplied by the Klein-Nishina cross section
μ	Total linear gamma ray attenuation coefficient in air at STP, cm^{-1}
μ_a	Total energy absorption coefficient for air at STP, cm^{-1}
μ_c	Total energy absorption coefficient for floor materials, cm^{-1}
$\vec{\xi}_i$	Direction of incident gamma ray
$\vec{\xi}_r$	Direction of reflected gamma ray
ρ	Distance from any point of an infinite plane isotropic source of radiation to the detector, feet
ρ'	Distance from a unit area dA to the perpendicular from the detector to the source plane, feet
$\bar{\rho}$	Distance from a point (x,y) in the ceiling to the detector in the building, feet
ϕ	Azimuthal angle of reflection, radians
ϕ'	Total change in azimuth between directions of incident and emergent gamma ray defined by Eq. (22), radians
ϕ_0	Azimuthal angle of incidence, radians
ϕ_1, ϕ_2	Azimuthal limits of the aperture, radians
χ	Dummy variable in x-integration

ψ	Dummy variable in ϕ-integration
ω	Solid angle fraction
$\bar{\omega}$	Dummy variable of integration over polar angles
ω_o	Cosine of incident polar angle
Ω	Solid angle, steradians

1.0 INTRODUCTION

Radioactive fallout is observed whenever a nuclear weapon is exploded. Because fallout contains radioactive atoms, and thus emits nuclear radiations that can cause damage in the cells of living tissue, the presence of fallout is usually equated with a potential radiological hazard to living matter. It is not surprising, therefore, that great concern has been devoted to the problem of fallout radiation exposure and that, in particular, many investigations have been made in the effort to determine the ability of existing or proposed structures to offer protection against fallout radiation.

Because of the rapid change of the absolute radiation intensity inside a structure following a fallout-producing event, it is not realistic to determine the absolute dose rate (1); rather it has become customary to measure the radiation protection afforded by a given structure in terms of a "standard unprotected position". The ratio of the dose rate at a given position in a structure to the dose rate in the unprotected position is commonly called the "reduction factor". The reciprocal of the reduction factor is called the "protection factor".

The standard unprotected position is presently defined as a detector location three feet above a hypothetical source of radiation of the same character as the fallout on the ground. The fallout is presumed to lie on a perfectly smooth, infinite plane. The ground is assumed to be replaced by compressed air of the same density, so that accurate theoretical analysis can be made (2). The reference dose rate can be calculated to within two to three percent accuracy, given the spectrum and strength of the fallout field. A commonly accepted value of the reference dose rate for a plane contaminated with one curie per square foot of Cobalt-60 is 485 roentgens per hour (3).

Several methods (2,4,5,6) are currently available for estimating the reduction factor of structures. There is a continuing trend toward individual consideration of each contributing factor thus increasing the reliability of the reduction factor concept. In the methods mentioned above, radiation which scatters from the ceiling is not considered as a separate contributing factor to the total radiation received at a point in the structure, but is lumped with the air scattered contribution into a single skyshine term. This term is then considered in conjunction with direct and wall scattered radiation for estimating the ground contribution from a field of fallout radiation.

There are instances, however, where ceiling scattered radiation, "ceiling-shine", does make a significant contribution to the total radiation, at times exceeding skyshine; for example, in buildings with a high band of windows and a roof overhang which cuts out skyshine.

The intent of this thesis was to undertake a systematic analytical investigation of the problem of ceiling-scattered radiation, trying, insofar as possible, to be consistent with the Engineering Method described in reference 4, so that the results from this work could eventually be incorporated in the above method. To this end the nomenclature used in (4) was followed wherever and whenever possible.

FORTRAN programming was employed throughout this study, utilizing the IBM-1410 facilities at the Kansas State University Computing Center and the CDC-3600 facilities at the Argonne National Laboratory Computing Center.

This thesis considers a multistory structure with windows. The size of the structure, as well as the percentage aperture and position of the windows, are varied. Ceilings are assumed to be semi-infinite reflective media and fallout is assumed to be uniformly distributed horizontally over exposed

surfaces. This is a standard assumption made in virtually all treatments of structure shielding against fallout radiation. The theoretical model is also based on the two following assumptions: 1) the dose angular distribution of radiation at the ceiling is not affected by the presence of the structure in the infinite field of radiation, and 2) the walls of the structure have zero linear thickness, yet are completely opaque to incident radiation.

Radioactive fallout consists of both fission fragments and neutron activated materials. The fission fragments constitute about 95% of the total radioactivity at one hour after a fission explosion (3). The fallout radiation energy spectrum changes with time. This feature comes about because of the different decay rates of the many radionuclides present in the fallout. Because of the time variation of the gamma-ray fission spectrum, it was necessary to make some decision regarding the choice of a spectrum to be utilized in this study (Appendix A).

The energy spectrum from fission at 1.12 hours after fission, with the volatile components removed, was chosen for three main reasons: (a) the spectrum at this time is representative of the spectra at earlier times, and most of the exposure to radiation is apt to occur during the first few hours, (b) volatile components would to a great extent remain separated from the fallout material, and (c) the penetration properties of fallout are, except for very large penetrations, not very sensitive to spectral changes (2). This spectrum is shown in Figure 1.

Utilization of this spectrum for all calculations would have required an inordinate amount of computer time; thus a few situations were analyzed, making use of the spectrum, and compared with results obtained for the same situations but using an infinite field of Cobalt-60 radiation (average energy

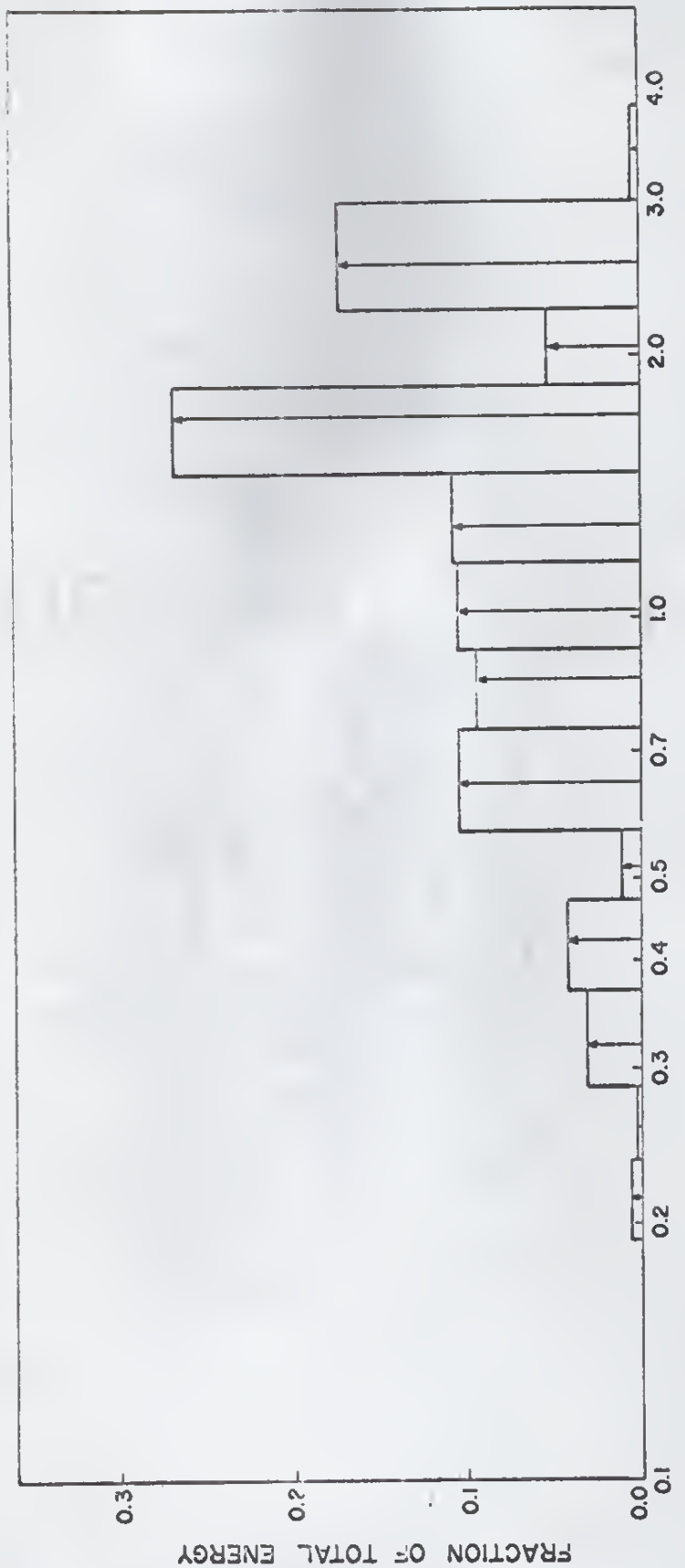

Figure 1. 1.12 hour fission spectrum.

1.25 Mev). The purpose of these calculations was to ascertain how well the use of a Cobalt-60 field of radiation would simulate an infinite field of fallout radiation. By such comparison it is possible to establish some criterion whereby results obtained by using Cobalt-60 radiation can be corrected to obtain the equivalent results, had an infinite fallout field been used. It was found (Appendix C) that an infinite field of Cobalt-60 radiation simulated the infinite field of fallout radiation with sufficiently good accuracy (five percent on the average), thus a Cobalt-60 infinite field of radiation was subsequently used for all remaining calculations.

2.0 THEORETICAL DEVELOPMENT

2.1 Derivation of Ceiling Shine Equation

The geometrical model utilized for the evaluation of the ceiling shine reduction factor is illustrated in Figure 2. This figure represents an idealized ith floor of a multistory building. The parameter d is the elevation of the ith ceiling above the source plane while d' is the distance between the ceiling and the floor. The surface of the first floor is considered to be in the source plane. Each floor contains a single window, not necessarily located centrally either horizontally or vertically in the wall. A combination of cartesian and polar coordinates is employed. The spherical coordinates of the window are represented in rectangular coordinates through the following transformations.

$$\phi_1 = \tan^{-1}[(x+D-R)/y] + \pi \tag{1}$$

$$\phi_2 = \tan^{-1}[(x+D+R)/y] + \pi \tag{2}$$

$$\theta_1 = \tan^{-1}\{[y/\cos(\phi_0-\pi)]/(H+V)\} \tag{3}$$

$$\theta_2 = \tan^{-1}\{[y/\cos(\phi_0-\pi)]/(H-V)\} \tag{4}$$

where V is the half-height of the aperture,

R is the half-width,

H is the distance from the center of the aperture to the ceiling, and

D is the offset of the aperture from the wall centerline.

Solution of the time independent Boltzmann equation for a plane source of radiation in an infinite homogeneous medium isotropically emitting one photon per unit area per unit time of energy E_0, yields a differential photon flux dependent on position, energy and direction. This flux,

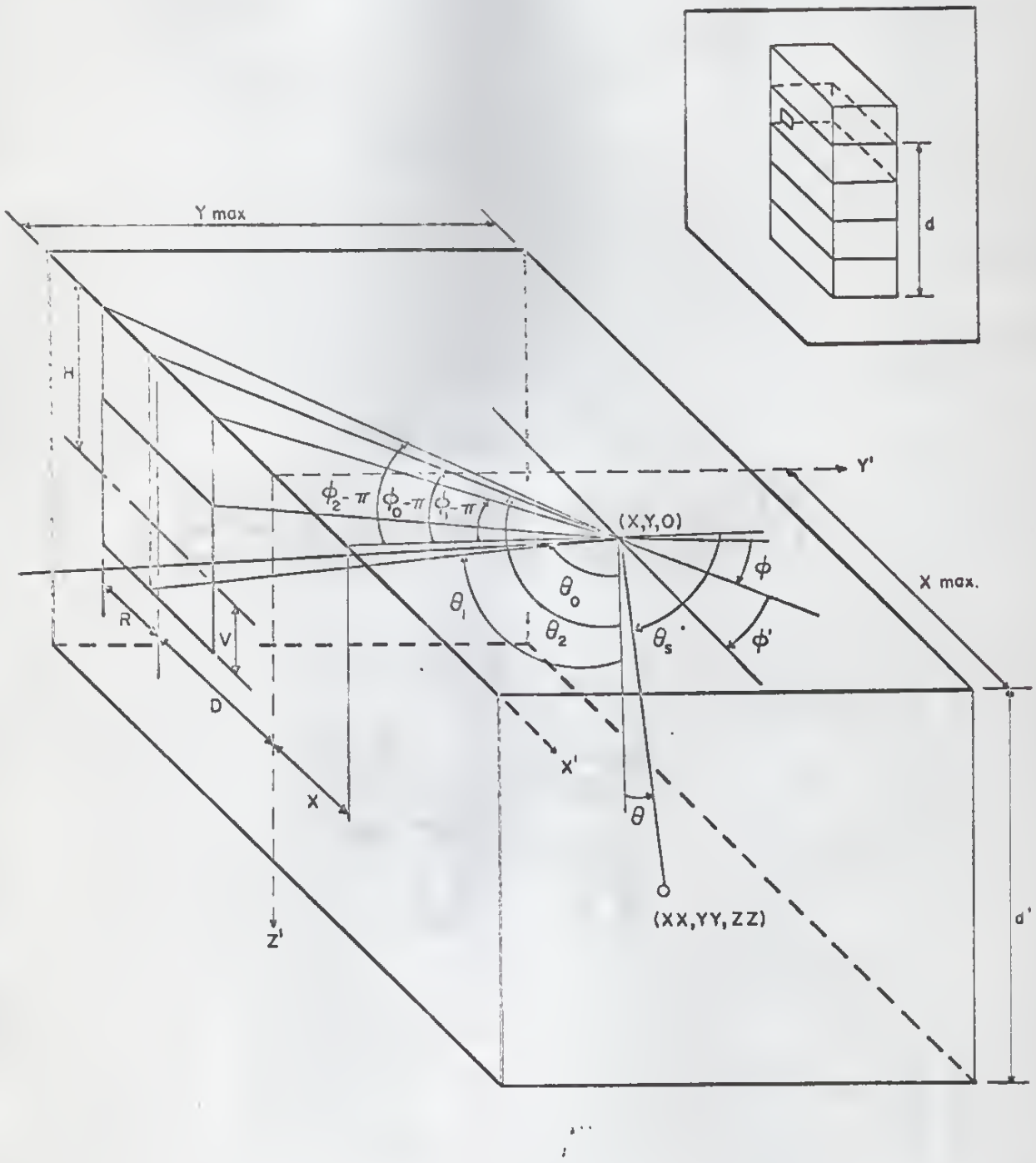

Figure 2. Schematic diagram of the ith floor of a multistory building.

$N_{pli}(d,E,\phi,\theta)dE\sin\theta d\theta d\phi$, represents the number of photons per unit area per unit time, with energies in dE about E, and direction θ and ϕ in the solid angle $\sin\theta d\theta d\phi$, where the unit area under consideration is normal to the direction θ and ϕ.

The exposure dose rate is proportional to the product of the flux N_{pli}, the energy E, and the energy absorption coefficient $\mu_a(E)$. The dose angular distribution for the plane isotropic source is then

$$F_{pli}(d,\theta,\phi) = \frac{1}{\alpha}\int_0^{E_o} \mu_a(E)\, E\, N_{pli}(d,E,\phi,\theta)\, dE \qquad (5)$$

where α is the conversion factor needed to give the resultant distribution units of exposure dose rate.

By definition,

$$\ell'(d,\theta,\phi) = F_{pli}(d,\theta,\phi)/D_o \qquad (6)$$

where D_o is the dose rate at the standard unprotected position, of Eq. (73) in Appendix C. Integrating over all azimuthal angles yields

$$\ell(d,\cos\theta_o) = 2\pi\, \ell'(d,\cos\theta_o,\phi_o). \qquad (7)$$

The dose angular distribution of radiation, $\ell(d,\cos\theta_o)$, from a cobalt-60 plane isotropic source has been calculated by Spencer (2) and is shown in Figure 3. It can be noted from this figure that for small penetrations, the dose angular distribution is sharply peaked in directions parallel to the source plane. This results in the high penetrability of the cobalt-60 (or fallout) radiation through vertical barriers. As the distance from the source plane is increased, however, the distribution becomes less sharply

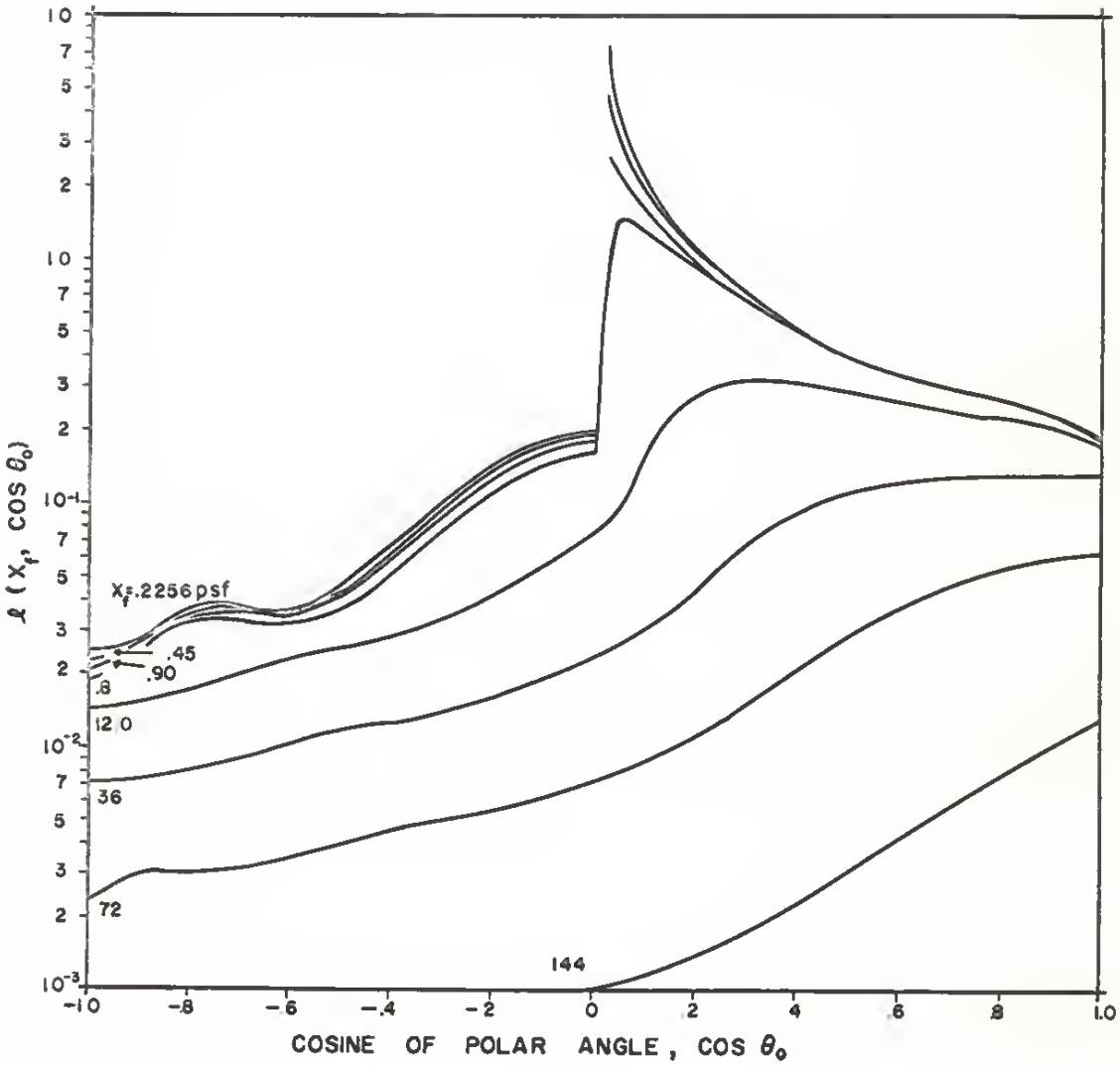

Figure 3. Dose angular distribution for cobalt-60 and concrete. (2)

peaked as the scattered component becomes increasingly dominant. Indeed, for great penetrations, the distribution becomes peaked at $\cos\theta_0 = 1$ (i.e., the oblique component is removed). The ordinate of Figure 3 is fixed so that an isotropic detector registering D_0 roentgens per hour at the standard unprotected position, registers

$$dD' = (D_0/2\pi)\ell(d,\cos\theta_0)\ \sin\theta_0 d\theta_0 d\phi_0 \tag{8}$$

due to photons striking it from directions within the solid angle $\sin\theta_0 d\theta_0 d\phi_0$. For reasons of economy of computer time and storage, it was necessary to represent $\ell(d,\cos\theta_0)$ by an analytical function. Implicit in $\ell(d,\cos\theta_0)$ is dependence on the energy E_0 of the source of radiation. Furthermore, for this work, d is a fixed parameter. Spencer (2) has pointed out that, when unscattered photons predominate (such as, near the source plane), $\ell(d,\cos\theta_0)$ resembles $(\cos\theta_0)^{-1}\exp(-a/\cos\theta_0)$, where a is a constant (dependent on the source photon energy and the height d). Referring now to the development in Appendix C, particularly Eq. (78), we choose to represent $\ell(d,\cos\theta_0)$ by the approximating function:

$$\ell(d,\cos\theta_0) = W(E_0,d,\cos\theta_0)B(E_0,d,\cos\theta_0)(\cos\theta_0)^{-1}\exp[-\mu(E_0)d/\cos\theta_0] \tag{9}$$

where, as noted, $\ell(d,\cos\theta_0)$ is implicitly a function of E_0. $B(E_0,d,\cos\theta_0)$ is the dose buildup factor for a point isotropic source:

$$B(E_0,d,\cos\theta_0) = 1 + a'(E_0)\mu(E_0)d(\cos\theta_0)^{-1}\exp[b(E_0)\mu(E_0)d/\cos\theta_0]. \tag{10}$$

$a'(E_0)$ and $b(E_0)$ are parameters for the build-up factor approximation of Chilton, Holoviak, and Donovan (7). These parameters depend on the composition of the medium, and are shown in Figure 4.

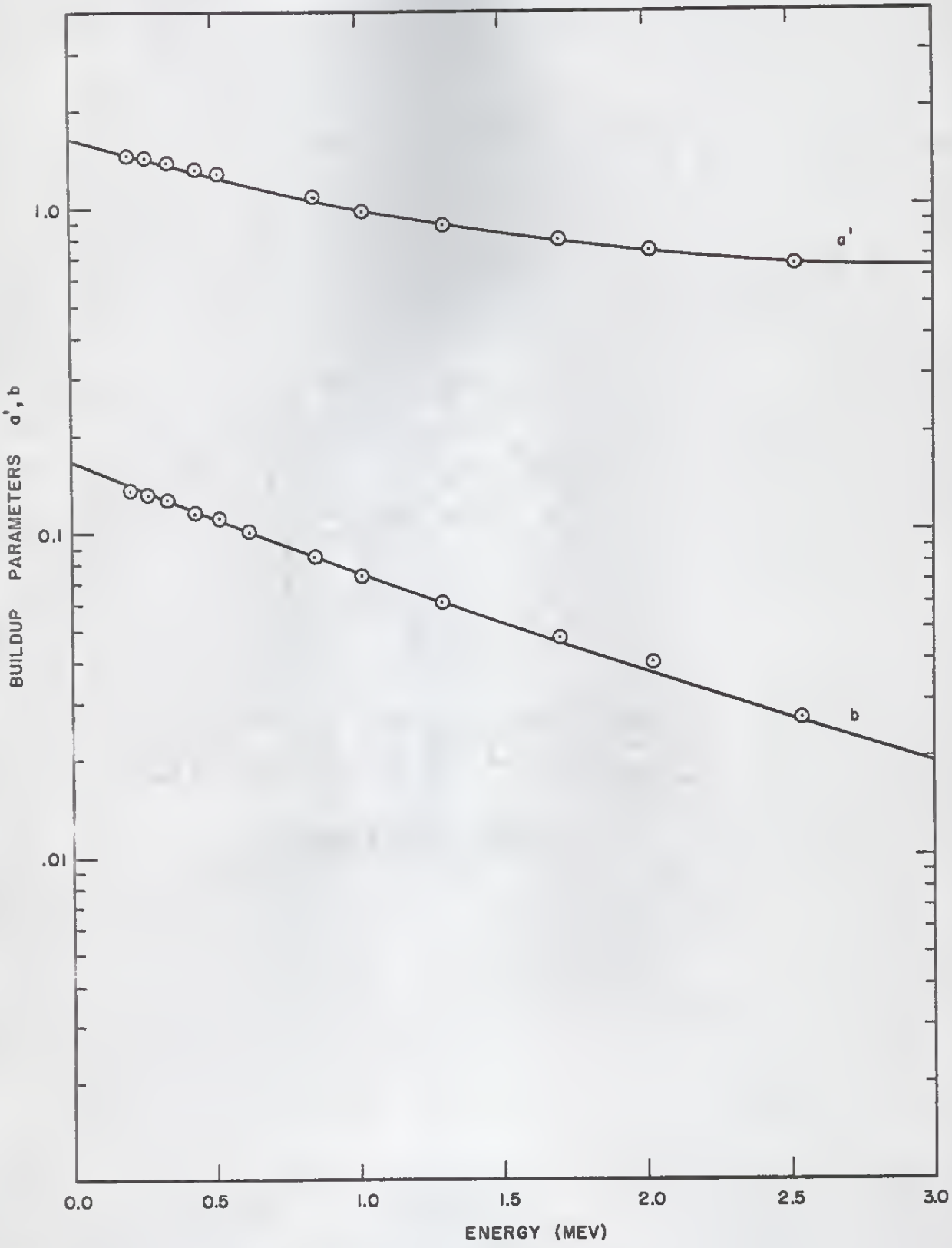

Figure 4. Build-up parameters a' and b as function of energy.

As it is pointed out in Appendix C, Eq. (78) is, at best, a very crude approximation to the dose angular distribution, and applies only to the range $0 < \cos\theta_0 < 1$. It was therefore necessary to include another factor $W(E_o,d,\cos\theta_0)$ in the approximation to the dose angular distribution. The following linear function of $\cos\theta_0$ was found to be satisfactory:

$$W(E_o,d,\cos\theta_0) = A(E_o,d) + B'(E_o,d)\cos\theta_0. \tag{11}$$

Again, E_o and d are parameters, rather than independent variables.

Since $\mu(E_o)$, $a'(E_o)$ and $b(E_o)$ were known, it remained only to determine $A(E_o,d)$ and $B'(E_o,d)$ by least-squares fitting of data from Figure 3. This analysis is described in Appendix A of reference 1.

The expression for the total incident dose rate at any point (x,y) on the ceiling utilizing Eqs. (1) through (4) is

$$D_i(x,y) = \frac{D_o}{2\pi}\int_{\phi_1}^{\phi_2}\int_{\theta_1}^{\theta_2}(A + B'\cos\theta_0)\ \frac{e^{-\mu(E_o)d/\cos\theta_0}}{\cos\theta_0} + \frac{a'\mu(E_o)d\ e^{(b-1)\mu(E_o)d/\cos\theta_0}}{\cos^2\theta_0}\ \sin\theta_0 d\theta_0 d\phi_0. \tag{12}$$

Before proceeding with the development of the theoretical ceiling shine equation, it is interesting to observe that an equation similar to equation (12) can be obtained from "point kernel theory".

The total incident dose rate at the ceiling is proportional to the photon flux above an infinite plane isotropic source of photons. The unscattered flux from a plane isotropic source emitting one photon per unit area per unit time is given by

$$F_u(d) = \int_{Area} \frac{e^{-\mu(E_0)R_0}}{4\pi R_0^2}\, dA. \tag{13}$$

The total flux is the product of the proper build-up factor and the uncollided flux of Eq. (13),

$$\text{i.e.,}\quad F(d) = \int_{Area} [1 + a'\mu(E_0)R_0\, e^{b\mu(E_0)R_0}][4\pi R_0^2\, e^{\mu(E_0)R_0}]^{-1}\, dA. \tag{14}$$

From the geometry of Figure 5,

$$R_0 = d/\cos\theta_0\ , \quad dA = R_0 dR_0 d\phi_0 \tag{15}$$

so that

$$F(d) = \frac{1}{4\pi}\int_{\phi_1}^{\phi_2} d\phi_0 \int_{\theta_1}^{\theta_2} \left[\frac{e^{-\mu d/\cos\theta_0}}{\cos\theta_0} + \frac{a'\mu d\, e^{(b-1)\mu d/\cos\theta_0}}{\cos^2\theta_0}\right] \sin\theta_0 d\theta_0. \tag{16}$$

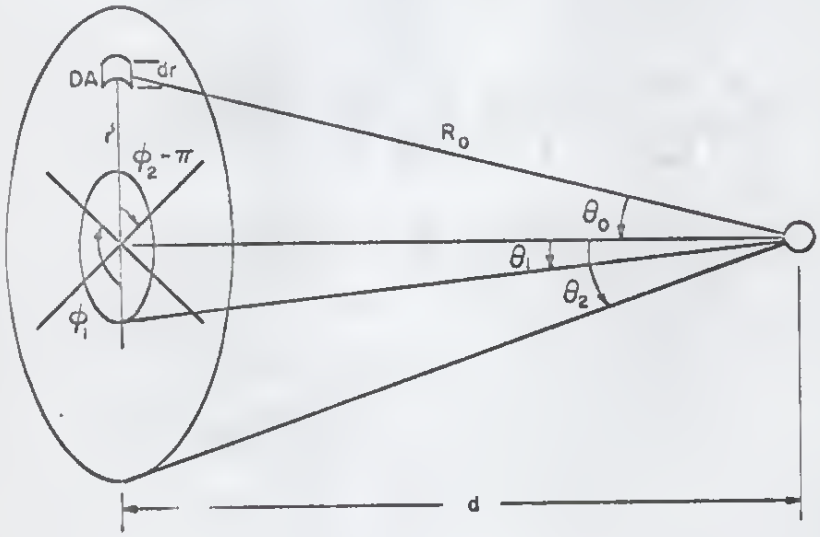

Figure 5. Plane surface source geometry.

Equations (12) and (16) are identical with the exception of the factor $(A + B' \cos\theta_0)$ which is included in Eq. (12) to permit a better empirical fit to the data from moments calculations (2) and a constant factor necessary to convert Eq. (15) from units of flux to dose.

The expression for the total incident dose rate at any point (x,y) on the ceiling is thus

$$D_i(x,y) = \frac{D_o}{2\pi} \int_{\phi_1}^{\phi_2} \int_{\theta_1}^{\theta_2} (A + B' \cos\theta_0) \quad \frac{e^{-\mu(E_o)d/\cos\theta_0}}{\cos\theta_0} + \frac{a'\mu(E_o)d \; e^{(b-1)\mu(E_o)d/\cos\theta_0}}{\cos^2\theta_0} \sin\theta_0 d\theta_0 d\phi_0. \tag{12}$$

In order to obtain the total reflected dose rate at the ceiling, it is necessary to define a reflection efficiency for the ceiling. This reflection efficiency is commonly designated as the "albedo". A differential dose rate albedo is used in this work (1). It is defined as the fraction of the dose rate incident on a surface at a given θ_0 and ϕ_0 which emerges from that surface into a solid angle $d\Omega$ about Ω. The albedo used in this work is a modification of one developed by Chilton and Huddleston (8,9,10).

The albedo used in Appendix C for the comparison of fission product results with the cobalt-60 results (1) is

$$\underline{a}(\theta_0,\phi_0;\theta,\phi) = 1.293 \cos\theta_0 [C\kappa(\theta_s) + C'](\cos\theta_0 + \cos\theta)^{-1}. \tag{17}$$

Here C and C' are the Chilton-Huddleston constants. Table I presents values for these constants at the thirteen energies of the fallout spectrum and at the cobalt-60 energy. The scattering angle θ_s can be obtained from the geometry of Figure 2, and the following consideration.

If $\vec{\xi}_i$ is the direction of the incident gamma ray, and $\vec{\xi}_r$ is the direction of the reflected ray, we can say that

$$\cos\theta_s = \vec{\xi}_i \cdot \vec{\xi}_r \tag{18}$$

From Figure 6 one can easily show that

$$\begin{aligned} \vec{\xi}_{i_x} &= + \sin\theta_0 \sin(\phi_0-\pi) \\ \vec{\xi}_{i_y} &= - \sin\theta_0 \cos(\phi_0-\pi) \\ \vec{\xi}_{i_z} &= - \cos\theta_0 \end{aligned} \tag{19}$$

and similarly

$$\begin{aligned} \vec{\xi}_{r_x} &= \sin\theta \sin\phi \\ \vec{\xi}_{r_y} &= \sin\theta \cos\phi \\ \vec{\xi}_{r_z} &= \cos\theta \end{aligned} \tag{20}$$

where $\vec{\xi}_x$, $\vec{\xi}_y$, $\vec{\xi}_z$ are the components of $\vec{\xi}$ in the x, y, and z directions.

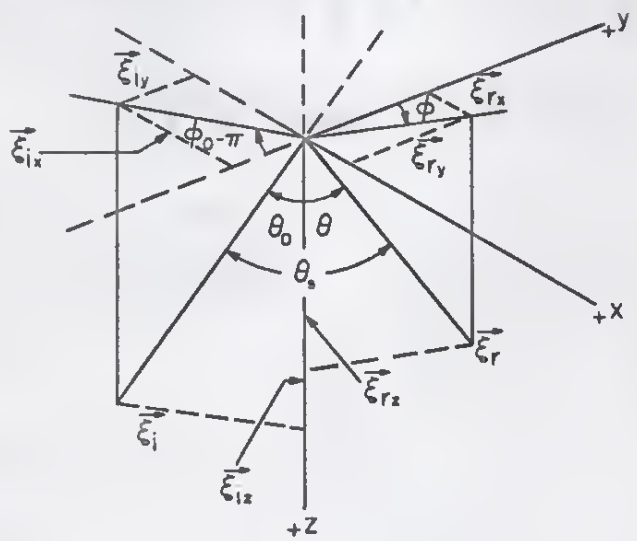

Figure 6. Coordinate system of albedo problem.

By substitution of Eq. (19) and Eq. (20) into Eq. (18) and carrying out the indicated dot product we conclude that

$$\cos\theta_s = \sin\theta \sin\theta_0 \cos\phi' - \cos\theta \cos\theta_0 \tag{21}$$

where

$$\phi' = \phi - \phi_0 + \pi. \tag{22}$$

Table I. Values of C and C' as a function of the incident radiation energy (9).

Energy (Mev)	C	C'
0.2128	0.003369	0.071531
0.2354	0.006860	0.064591
0.3193	0.011891	0.054976
0.4257	0.019726	0.041085
0.5108	0.025504	0.031879
0.6386	0.033366	0.021235
0.8514	0.043641	0.014983
1.0217	0.051245	0.011373
1.2520	0.060872	0.007439
1.2772	0.061879	0.007075
1.7029	0.077531	0.002897
2.0435	0.086038	0.006731
2.5545	0.101482	0.004928
3.4059	0.124210	0.002916

The parameter $\kappa(\theta_s)$ is p times the Klein-Nishina cross section where

$$p = \{1 + E_o(1 - \cos\theta_s)/0.511\}^{-1}. \quad (E_o \text{ in Mev}) \tag{23}$$

While Eq. (17) was used for all the calculations in Appendix C, a still more accurate formula was used to evaluate the required data for the design curves

This formula is

$$\underline{a}(\theta_0;\theta,\phi) = 1.293 \cos\theta_0 \frac{F_a(\theta_0,\theta,\phi)[C\kappa(\theta_s) + C']}{\cos\theta + (\cos\theta_0 \sqrt{1 + 2\,E_0(1-\cos\theta_s)})}, \qquad (24)$$

where

$$F_a(\theta_0;\theta,\phi) = A_1 + A_2(1 - \cos\theta_0)^2 + A_3(1 - \cos\theta)^2 + A_4(1 - \cos\theta_0)^2(1 - \cos\theta)^2 + A_5(1 - \cos\theta_0)(1 - \cos\theta)(1 - \cos\phi). \qquad (25)$$

The values of the constants in Eqs. (24) and (25) are presented in Table II.

Table II. Values of albedo parameters.

Parameter	Cesium-137 (0.662 Mev)	Cobalt-60 (1.25 Mev)
C	0.0455	0.0710
C'	0.0161	0.0114
A_1	1.512	1.555
A_2	-0.606	-0.629
A_3	-0.641	-0.605
A_4	0.645	0.539
A_5	-0.157	-0.168

An experimentally determined albedo equation (11) was considered. However, its limited range, especially in the incident polar angle, precluded its use in this work. Combining Eqs. (12) and (24) yields the differential reflected dose rate at any point (x,y) of the ceiling.

$$\text{i.e.,}\quad D_r(x,y;\theta,\phi)\,\sin\theta d\theta d\phi = \frac{1.293}{2\pi} D_0 \int_{\phi_1}^{\phi_2} d\phi_0 \int_{\theta_1}^{\theta_2} d\theta_0 (A + B' \cos\theta_0)$$

$$\left[\frac{e^{-\mu d/\cos\theta_0}}{\cos\theta_0} + \frac{a'\mu d\, e^{(b-1)\mu d/\cos\theta_0}}{\cos^2\theta_0}\right] [F_a(\theta_0;\theta,\phi)][C\kappa(\theta_s) + C'] \qquad (26)$$

$$\times \left[\cos\theta + \cos\theta_0 \sqrt{1 + 2E_0(1-\cos\theta_s)}\right]^{-1} \cos\theta_0 \sin\theta_0 \sin\theta d\theta d\phi.$$

This differential reflected dose rate can be thought of as a plane source of gamma radiation with strength varying with ceiling position and emergent polar (θ) and azimuthal (ϕ) angles.

For a ceiling located at an elevation d, the distance from a point (x,y) on the ceiling to the detector located at a point (xx,yy,zz) is given by

$$\bar{\rho} = [(xx-x)^2 + (yy-y)^2 + zz^2]^{1/2}. \qquad (27)$$

From the geometry of Figure 2, the emergent angles are given by the following relations:

$$\theta = \cos^{-1}(zz/\bar{\rho}) \qquad (28)$$

$$\phi = \tan^{-1}\left(\frac{xx-x}{yy-y}\right) + \pi. \qquad (29)$$

The dose received by an isotropically responding detector located at (xx,yy,zz) is

$$\bar{D} = \int_{\text{Area}} \frac{D_r(x,y;\theta,\phi)\cos\theta\, dx\, dy}{\bar{\rho}^2}. \qquad (30)$$

The reduction factor at a point (xx,yy,zz) in the structure can be obtained by dividing both sides of Eq. (30) by D_0, substituting Eq. (26) for $D_r(x,y;\theta,\phi)$, and integrating over the ceiling area. The equation for the total reduction

factor must incorporate attenuation and build-up terms to account for the media traversed by the reflected radiation prior to striking the detector (this could include floors or interior partitions). This results in the following equation for the reduction factor anywhere in a structure.

$$R.F.(xx,yy,zz) = \frac{1.293}{2\pi} \int_{-XMAX}^{XMAX} dx \int_{0}^{YMAX} dy \int_{\phi_1}^{\phi_2} d\phi_0 \int_{\theta_1}^{\theta_2} (A + B' \cos\theta_0)$$

$$\times \left[e^{-\mu(E_0)d/\cos\theta_0} + \frac{a'\mu(E_0)de^{(b-1)\mu(E_0)d/\cos\theta_0}}{\cos\theta_0} \right] F_a(\theta_0;\theta,\phi)[C\kappa(\theta_s) + C']$$

$$\times \cos\theta\{1 + a'[\mu(E)(\bar{\rho}-t/\cos\theta) + \mu_c t/\cos\theta]\exp[b(\mu(E)(\bar{\rho}-t/\cos\theta)$$

$$+ \mu_c(E)t/\cos\theta)]\}\{\exp[\mu(E)(\bar{\rho}-t/\cos\theta) + \mu_c(E)t/\cos\theta]\}^{-1} \qquad (31)$$

$$[\bar{\rho}^{-2}(\cos\theta + \cos\theta_0 \sqrt{1 + 2E_0(1-\cos\theta_s)})]^{-1}\sin\theta_0 d\theta_0$$

where $F_a(\theta_0;\theta,\phi)$ is given by Eq. (25),

t is the thickness of any floor between the ceiling in consideration and the detector, and

$\mu_c(E)$ is the total gamma-ray linear attenuation coefficient for the material of a floor between the ceiling and the detector.

This equation was solved numerically.

2.2 Transformation of Equations for Computer Utilization

An IBM-1410 digital computer, with 4000 word storage capacity, and a COC-3600 computer with 64,000 word storage capacity, were used alternatively for all machine calculations necessary in this thesis. FORTRAN IV and COC-FORTRAN languages were utilized.

The numerical technique known as Gaussian quadrature was employed to integrate Eq. (31). This technique and its accuracy are discussed in Appendix B. Gauss' mechanical quadrature formula is

$$\int_{-1}^{1} f(x)dx = \sum_{i=1}^{n} w_i \, f(u_i) \tag{32}$$

where w_i are the Christoffel numbers and u_i are the zeros of the Legendre polynomials. Values of w_i and u_i are tabulated for order n from 3 to 20 in Appendix B (12,13).

First the integration over the incident azimuthal angles is performed by application of Eq. (32). This is accomplished by letting

$$\phi_0 = \frac{1}{2} \left(\phi_2(x) - \phi_1(x)\right) \psi(x) + \frac{1}{2} \left(\phi_2(x) + \phi_1(x)\right) \tag{33}$$

$$d\phi_0 = \frac{1}{2} \left(\phi_2(x) - \phi_1(x)\right) d\psi(x) \tag{34}$$

Note that the limits of the integration $\phi_2(x)$ and $\phi_1(x)$ are directly dependent on x through Eqs. (1) and (2). Thus

$$\int_{\phi_1}^{\phi_2} d\phi_0 \, f(\phi_0) = \frac{\phi_2-\phi_1}{2} \int_{-1}^{1} d\psi \, f(\psi) = \frac{\phi_2-\phi_1}{2} \sum_{k=1}^{K} a_k \, f(\psi_k) \tag{35}$$

where the explicit dependence on x is tacitly assumed. Substitution in Eq. (31) will essentially remove the integration over the azimuthal angles, substituting in its place the right hand side of Eq. (35), and leaving everything else unchanged.

Since θ_0 always appears in the form $\cos\theta_0$, it is convenient before one integrates, to make a change in variables from θ_0 to ω_0, where

$$\omega_0 = \cos\theta_0 \tag{36}$$

Again we let

$$\omega_0 = \frac{1}{2}\left[\omega_2(y,\phi_0(\psi)) - \omega_1(y,\phi_0(\psi))\right]\bar{\omega}(y,\phi(\psi(x))) + \frac{1}{2}\left[\omega_2(y,\phi_0(\psi)) + \omega_1(y,\phi_0(\psi))\right] \tag{37}$$

$$\omega_2(y,\phi_0) = \cos\theta_2(y,\phi_0)$$
$$\omega_1(y,\phi_0) = \cos\theta_1(y,\phi_0) \tag{38}$$

The explicit dependence of θ_1 and θ_2 on y and ϕ_0 is given by Eqs. (3) and (4), and ϕ_0 itself is explicitly dependent on ψ and x, as shown in Eq. (33)

$$d\omega_0 = -\frac{1}{2}\left[\omega_2(y,\phi_0(\psi)) - \omega_1(y,\phi_0(\psi))\right] d\bar{\omega}(y,\phi_0(\psi(x))) \tag{39}$$

$$\int_{\omega_1}^{\omega_2} d\omega_0\ f(\omega_0) = \frac{\omega_1-\omega_2}{2}\int_{-1}^{1} d\bar{\omega}\ f(\bar{\omega}) = \frac{\omega_1-\omega_2}{2}\sum_{j=1}^{K} a_j\ f(\bar{\omega}_j) \tag{40}$$

where, again, the arguments indicating the explicit dependence of each variable have been deleted for simplicity.

The y and x integration are now performed by the usual changes

$$y = \frac{1}{2}\,\mathrm{YMAX}\cdot\tilde{y} + \frac{1}{2}\,\mathrm{YMAX} \tag{41}$$

$$dy = \frac{1}{2}\,\mathrm{YMAX}\,d\tilde{y} \tag{42}$$

$$\int_{0}^{\mathrm{YMAX}} dy\ f(y) = \frac{\mathrm{YMAX}}{2}\int_{-1}^{1} d\tilde{y}\ f(\tilde{y}) = \frac{\mathrm{YMAX}}{2}\sum_{m=1}^{M} a_m\ f(\tilde{y}_m) \tag{43}$$

ano

$$x = \frac{1}{2}\,(XMAX + XMAX)\,x \tag{44}$$

$$dx = XMAX\ dx \tag{45}$$

$$\int_{-XMAX}^{XMAX} dx\ f(x) = XMAX \int_{-1}^{1} dx\ f(x) = XMAX \sum_{c=1}^{L} a_c\ f(x_c) \tag{46}$$

so that finally the equation for the total reduction factor at a point (xx, yy,zz) in a structure becomes

$$R.F.(xx,yy,zz) =$$

$$\frac{1.293}{16\pi}\ YMAX \cdot XMAX \cdot \sum_{c=1}^{L} a_c\ [\phi_2(x_c) - \phi_1(x_c)] \sum_{m=1}^{M} a_m \sum_{k=1}^{K} a_k$$

$$\cdot\ [\omega_1(\tilde{y}_m,\phi_0(\psi_k(x_c))) - \omega_2(\tilde{y}_m,\phi_0(\psi_k(x_c)))] \sum_{j=1}^{K} a_j\ F(x_c,\tilde{y}_m,\omega_j,\psi_k) \tag{47}$$

where $F(x_c,\tilde{y}_m,\omega_j,\psi_k)$ is the integrand of Eq. (31) after the indicated changes in the inoependent variable ω_0 have been performed.

3.0 RESULTS OF CALCULATIONS

3.1 The Design Curves

3.1.1 Development of the Design Curves

Figure 2 illustrates many of the parameters that must be taken into consideration in calculations leading to sets of curves for determining the ceiling shine reduction factor in a structure. These parameters can be classified into four groups: ceiling parameters, window parameters, detector parameters, and energy parameters. While the first three types have a geometrical nature in that they only relate to the geometrical arrangement and dimensions of the structure, the energy parameters arise indirectly from the treatment of the fallout field as a superposition of monoenergetic sources. These energy parameters are considered in great detail in Appendix C. These four groups can be further defined as follows.

A. Ceiling parameters: Those relating to the size of the structure and the height of the ceiling above the source plane. There are four parameters of this type.
   1) XMAX, defined as half the length of the wall in which the window is located,
   2) YMAX, the total length of the adjacent wall,
   3) d, the height of the ith ceiling above the source plane, and
   4) t, the thickness of each floor slab.

B. Window parameters: Describe the location and dimension of the window. There are four parameters of this type.

1) H, the distance of the window horizontal centerline from the ceiling,
2) V, the half height of the window (these first two parameters determine the sill height and upper level of the window),
3) R, the half width of the window, and
4) D, the offset of the window vertical centerline from the wall centerline.

C. Detector parameters: Relate to the position of the detector with respect to the ceiling.

1) xx, the x coordinate of the detector,
2) yy, the y coordinate of the detector, and
3) zz, the z coordinate of the detector.

D. Energy parameters: Do not enter directly into the calculation of the reduction factor in a structure exposed to fallout radiation, in that, as was previously stated, it is possible to simulate the fallout field with an infinite field of monoenergetic cobalt-60 radiation. Energy parameters are, however, used in verifying the accuracy of simulating the infinite field of fallout radiation with a field of cobalt-6D radiation.

It should be pointed out that, while physical dimensions are used directly in the calculations for the design curves, they do not necessarily appear as parameters in the sets of curves themselves. It becomes more convenient, in the presentation of these curves, to utilize some other parameters, (e.g.,

solid angle fraction, eccentricity, percentage aperture, etc.) which are functions of the geometrical parameters.

The building eccentricity, E, is defined as the ratio of the dimension of the side in which the window is located (2 x XMAX) to the dimension of the adjacent side (YMAX). It is not the ratio of the smaller to the larger side of the building as given in reference 4.

The fraction of solid angle subtended by the ceiling at the detector is a function of the ceiling dimensions and the perpendicular distance from the ceiling to the detector. The equation for the solid angle fraction (2) is given by

$$\omega(\varepsilon,\eta) = \frac{2}{\pi} \tan^{-1} \frac{\varepsilon}{\eta(1+\varepsilon^2+\eta^2)^{1/2}} \tag{48}$$

where $$\varepsilon = W/L \quad \text{and} \quad \eta = 2(zz)/L. \tag{49}$$

The function $\omega(\varepsilon,\eta)$, plotted in Figure 41.2 of the Engineering Manual (4), is reproduced as Figure 8. The percentage aperture of one wall is the ratio of ten feet times the width of the window to the area of the wall plus the window.

Not all values of the eleven physical parameters discussed above were used in the calculation of design curves for determining the ceiling scattered reduction factors. As each of the parameters could assume a large number of values, this would have required an inordinate amount of time on the digital computers employed (CDC-3600 and IBM-1410). Preliminary studies were conducted to ascertain the relative importance of each of the parameters. Final calculations were performed for various selected geometrical situations which provided a sufficient representation of the reduction factor variation. Table III summarizes the values of various parameters employed in the calculations. All

possible combinations of the parameters listed in this table were utilized except for ceiling heights different from thirteen feet and sill heights other than three feet, only five of the percentage apertures and two of the sill heights were employed.

Table III. Design curve parameters.

Ceiling height above source plane (feet)	13			39		65			91	
Ceiling Width, W (feet)	10			20		30		50		100
Ceiling Length, L (feet)	10			20		30		50		100
Sill height (feet)	3		5		7	8	9		10	11
Percentage Aperture (%)	5	10	15	20	30	40	50	60	70	76.9*

* This is the maximum possible percentage aperture with thirteen foot high rooms and three foot sill heights (i.e., 10/13 = 0.769).

The design curves are presented in Figures 7, 8, 9, 10, 10a, and 11.

Following is a brief description of the procedure used to develop these curves. Solutions of Eq. (31) for different size square buildings were plotted directly to obtain Figure 7.

The procedure employed in obtaining the eccentricity correction curve (Figure 9) follows.

1. The reduction factor in rectangular buildings was determined for different percentage apertures while holding the eccentricity constant.
2. For a given eccentricity and solid angle, the ratio of the reduction factor in the eccentric building to that in a square building was determined for each percentage aperture, and an average ratio calculated. A standard deviation was also calculated.

3. The average ratio (eccentricity factor) was plotted versus the eccentricity for which it was obtained.
4. The same procedure was repeated for different eccentricities.

To determine the sill height factor $R_s(\omega,h)$ for Figure 10, the following procedure was followed.

1. Several reduction factors were evaluated for a given structure by keeping the upper level of the window at ceiling height and the window width unchanged while allowing the window sill height to vary.
2. The ratios between the reduction factors obtained for each sill height to the reduction factor calculated with the sill height at three feet were plotted as function of the solid angle fraction.

The curves in Figure 11 were obtained by determining the ratio of the reduction factors obtained for identical geometrical situations at the given height to that at a height of thirteen feet.

3.1.2 Using the Oesign Curves

Because of the relatively large number of parameters involved in the calculation of a ceiling shine reduction factor, it was necessary to develop a set of curves for some standard structure. Correction factors are applied to the standard structure results to obtain reduction factors for other structures.

The standard structure was chosen to be the first floor of a square concrete building. A single window was located centrally in one of the walls with the sill height at three feet above the floor and the upper level flush with the ceiling. The detector was positioned three feet above the center of the floor. The distance between floor and ceiling was set at thirteen feet.

Eq. (31) was solved for standard structures ranging in floor area from 100 to 10,000 square feet. The resulting reduction factors are plotted for

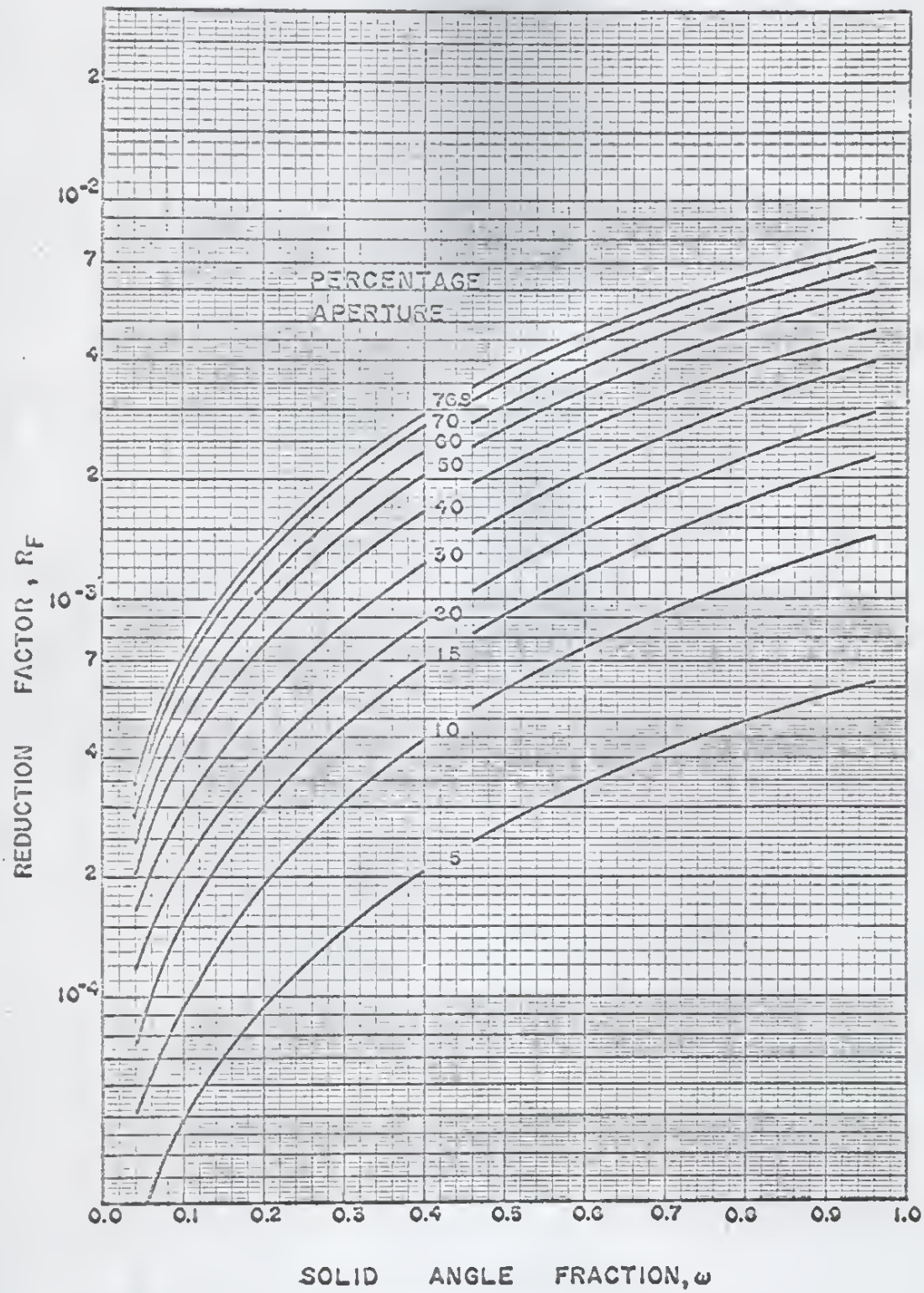

Figure 7. First floor reduction factor in a square building.

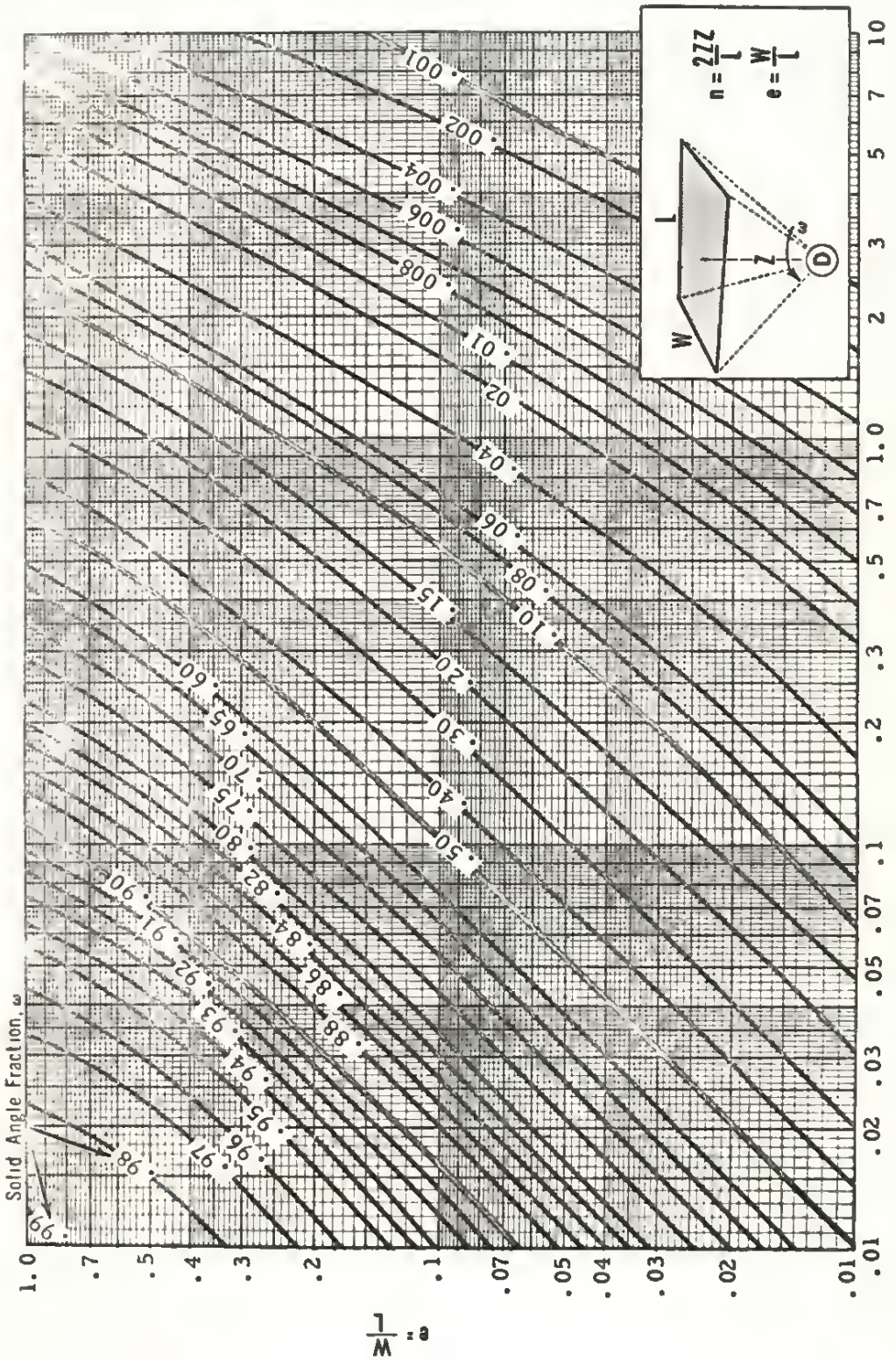

Figure 8. Solid Angle Fraction, ω

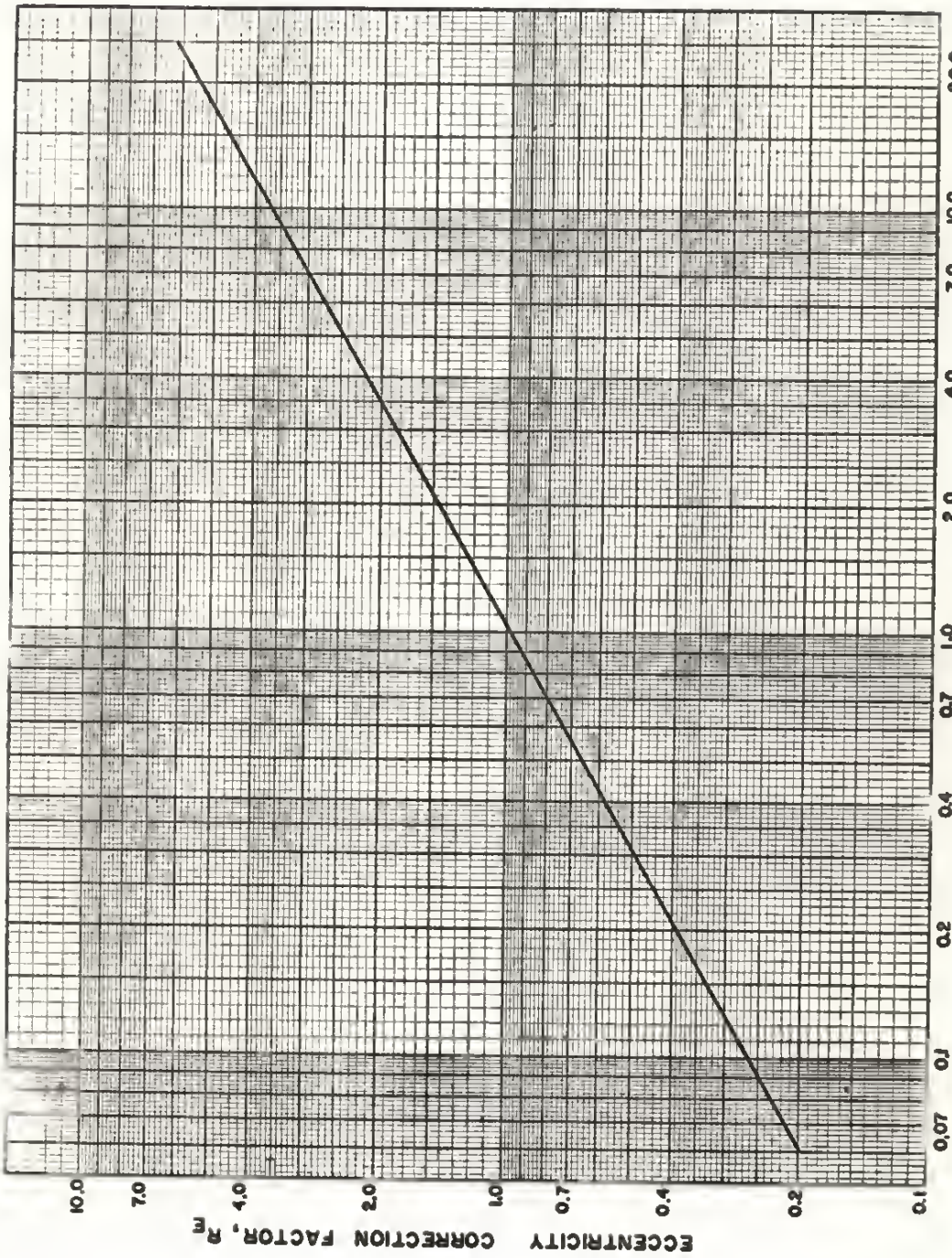

Figure 9. Eccentricity correction factor.

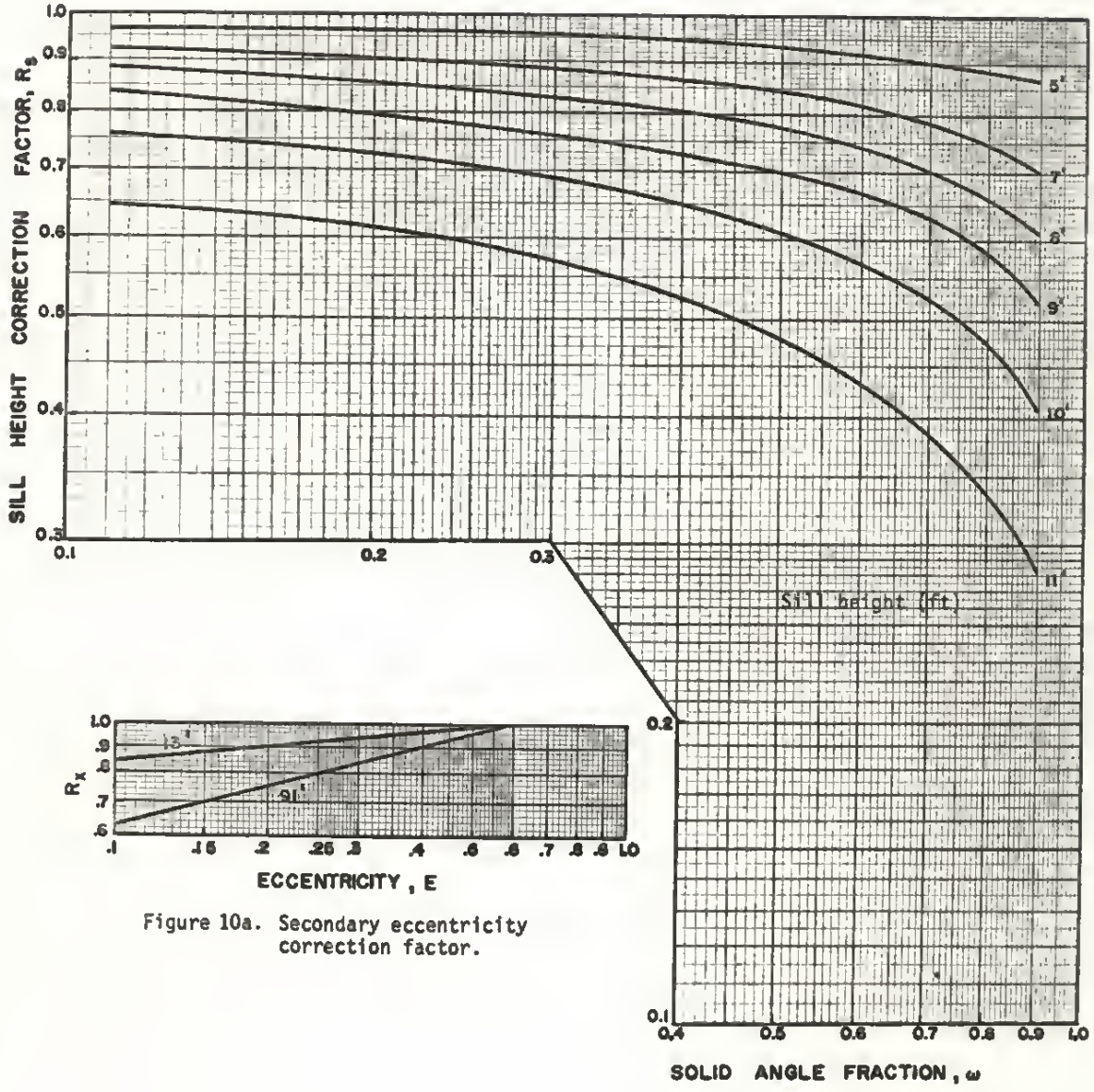

Figure 10a. Secondary eccentricity correction factor.

Figure 10. Sill-height correction factor.

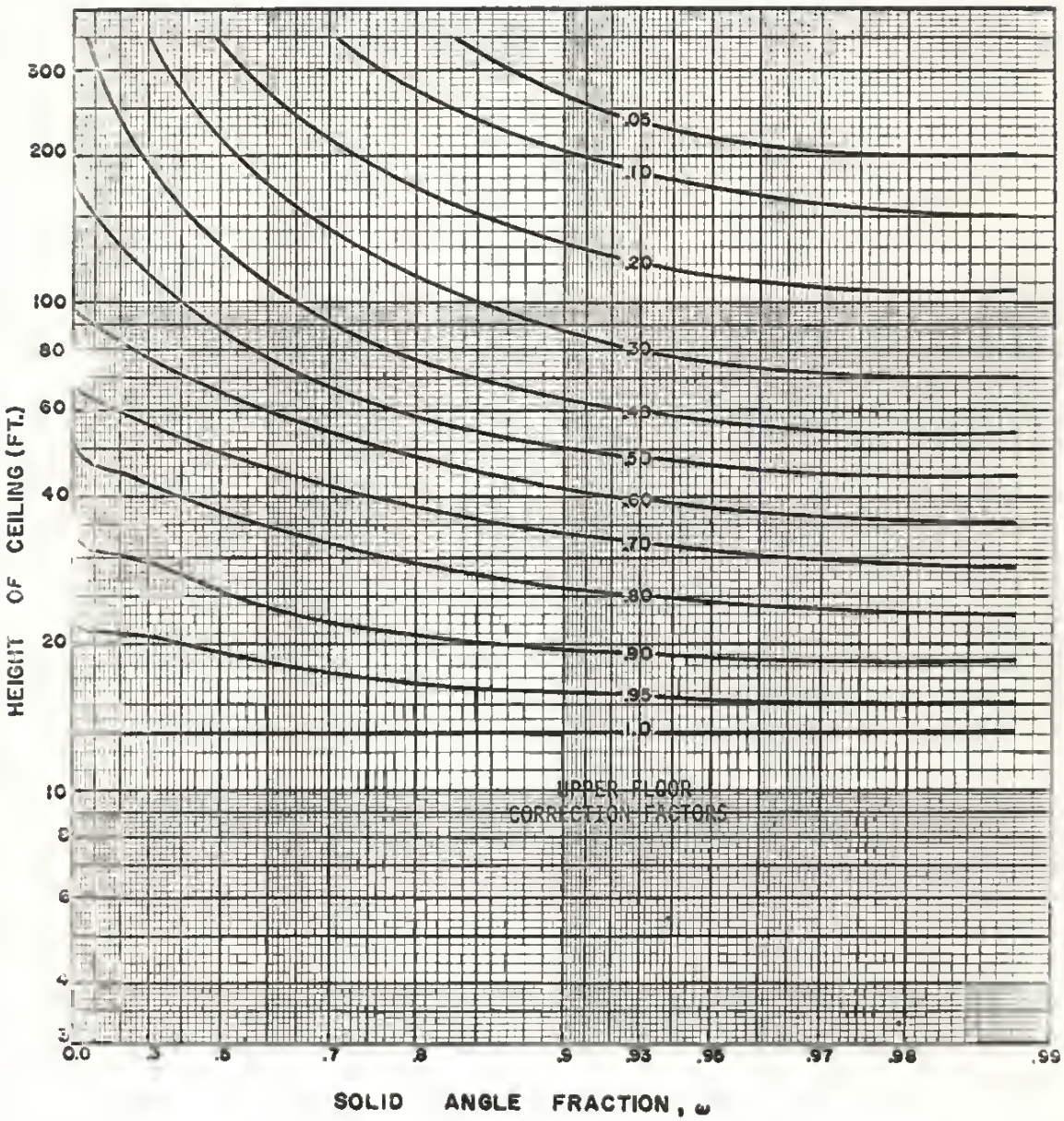

Figure 11. Correction factor for the detector positioned in upper stories, R_U.

different percentage apertures (ten feet times window width/window plus wall area for one wall) as functions of the fraction of solid angle subtended by the ceiling at the detector in Figure 7. The solid angle fraction may be obtained through the use of Figure 8 (chart 1 in reference 4).

The ceiling shine contribution in a rectangular building of equivalent ceiling area and percentage aperture may be obtained by multiplying the reduction factor for a square building taken from Figure 7 by the correction factor plotted in Figure 9. This correction is called the eccentricity correction factor. The eccentricity, E = W/S, is defined as the ratio of the length of the side containing the window to the adjacent side. Figures 7 and 9 used together will therefore yield the reduction factor three feet above the center of a rectangular building with a window of the same dimensions as that of the standard structure.

The reduction factor three feet above the center of the first floor of either a square or a rectangular building with windows located anywhere in the wall can be determined with the additional use of Figure 10.

The reduction factor three feet above the center of the floor of the structure in Figure 12 is given by Eq. (50),

$$\text{R.F.} = R_f(\omega,P)\, R_E(E)\, \{R_s(\omega,h_1) - R_s(\omega,h_2)\}, \tag{50}$$

where $R_f(\omega,P)$ is the reduction factor for a square building with percentage aperture P and solid angle fraction ω (Fig. 7),

$R_E(E)$ is the eccentricity factor (Fig. 9), and

$R_s(\omega,h)$ is the multiplicative correction factor for a sill height of h feet (Fig. 10).

A differencing technique can be used for windows located in off-center positions in one of the walls (Fig. 13). The general expression for the reduction

factor can be written as

$$R.F. = \frac{1}{2} R_L(E) \{R_s(\omega,h_1) - R_s(\omega,h_2)\} \{R_f(\omega,P_1) - R_f(\omega,P_2)\} \qquad (51)$$

where P_1 is the percentage aperture determined using R_1 as the window width,

and P_2 is the percentage aperture with R_2 as the window width.

The factor of one-half in Eq. (51) is introduced because the differencing technique yields the reduction factor for two identical windows symmetrically located about the wall centerline. If the windows are not symmetrical or are of different size, the reduction factor contributions must be evaluated for each of the windows and then added.

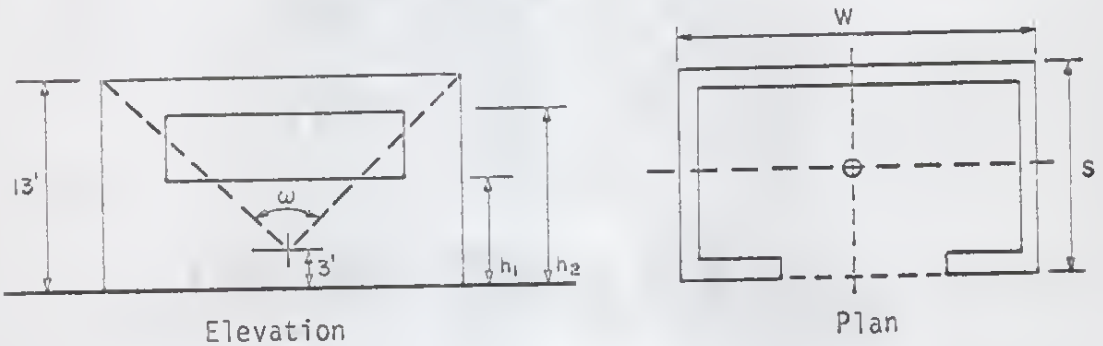

Figure 12. Sample structure describing Eq. (50).

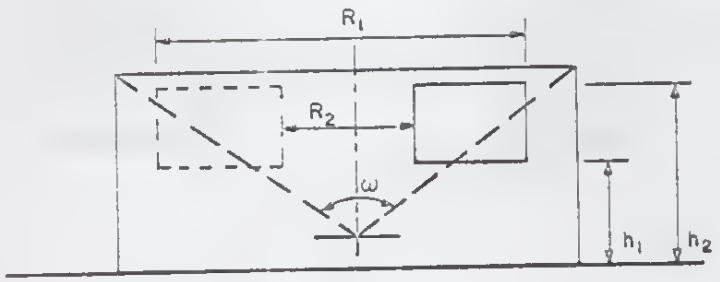

Figure 13. Structure used in description of Eq. (51) and (52).

Special attention must be paid to situations for which the window is located in the narrow side of the building (i.e., E<1.0). For such cases, the correction factor for sill height was found to have a value lower than that obtained from Figure 10. This can be attributed to a secondary eccentricity effect. For rectangular buildings with the window located in the narrow side, the main contribution from the ceiling to the reduction factor will originate from the very front of the building. Little contribution will come from the back. Thus the structure behaves as if it were actually of smaller size, and the reduction factor will be lower. Figure 10a provides the means of correcting for the added effect. This factor is termed $R_x(E)$.

The factor obtained from Figure 11 corrects for the reduction factors three feet above the center of the floor of upper stories. The additional correction factor $R_x(E)$ (Fig. 10a) must again be used whenever the reduction factor is calculated for rectangular buildings with eccentricities less than one.

With the geometry of Figure 13 for a ceiling at an elevation other than thirteen feet, the reduction factor can be determined from

$$\text{R.F.} = \frac{1}{2} R_x(E)\, R_E(E)\, R_u(\omega,d) \{R_s(\omega,h_1) - R_s(\omega,h_2)\} \{R_f(\omega,P_1) - R_f(\omega,P_2)\}, \tag{52}$$

where $R_x(E)$ is equal to 1.0 for $E \geq 0.6$ and

$R_u(\omega,13') = 1.0$.

The contribution from the floor above the detector floor can be approximately determined with the use of chart 1 in reference 14. Since the ceiling shine contribution is part of the general ground contribution, the correct

factor to be employed on this chart is $B_0'(X_0')$, defined as the ceiling barrier factor for the ground contribution. X_0' is the thickness of the floor slab in pounds per square foot (psf) and $B_0'(X_0')$ is equal to unity for a zero thickness floor slab.

The general expression which yields the ceiling shine contribution in the center of a structure is

$$\begin{aligned} \text{R.F.} = {} & \frac{1}{2} R_E(E)\, R_x(E)\, R_u(\omega_1, d_1) \{R_f(\omega_1, P_1) - R_f(\omega_1, P_2)\} \\ & \{R_s(\omega_1, h_1) - R_s(\omega_1, h_2)\} + \frac{1}{2} B_0'(X_0')\, R_E(E)\, R_x(E)\, R_u(\omega_2, d_2) \\ & \{R_f(\omega_2, P_1) - R_f(\omega_2, P_2)\} \{R_s(\omega_2, h_1) - R_s(\omega_2, h_2)\}. \end{aligned} \tag{53}$$

Equations (50) through (53) apply only to the case of a single window located in one of the walls. The calculation must be repeated for all windows located in the structure.

Although all design curves were based on a detector to ceiling distance of ten feet, they can still be used for other distances as long as the correct solid angle is utilized.

To better illustrate the use of the design curves, particularly in the case where the detector is not centrally located, some numerical examples are presented in the following pages.

The basic method for analyzing the ceiling shine contribution has been described for situations where the detector is assumed to be centrally located horizontally in a square or rectangular structure having only one window in one of the walls. In most actual buildings, however, there will be many windows present and the detector will not be symmetrically located. The following describes a procedure whereby the contribution due to ceiling shine can

evaluated for such cases.

2. Identical windows symmetrically located in each of the walls.

   i) Square buildings

   For the case of a single window located in each of the walls, the reduction factor is four times the contribution from one window only. If more than one window is located in each wall, the contributions from each of the windows in the wall are added and multiplied by four to obtain the total reduction factor. The analysis of a simple square structure with several windows equally spaced around the building is illustrated in Example 1. The plan and elevation of the structure are shown in Figure 14.*

Example 1

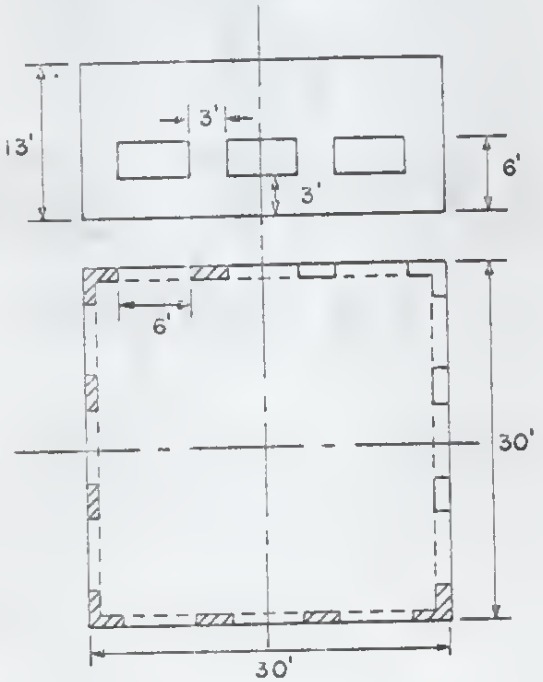

Figure 14. Structure elevation and plan for Example 1.

*In the following examples, for clarity, the plan views of buildings are shown in section through the windows.

Given the structure in Figure 14, the reduction factor three feet above the center of the floor must be determined. The contribution from each of the windows in one wall is obtained by a differencing technique. For all three windows, the contribution to the reduction factor is equal to the difference between the contribution obtained with the sill height placed at three feet (h_1) and that obtained with the sill height at six feet (h_2). To evaluate the contribution from the two outer windows a differencing technique must be further employed. The reduction factor contribution is computed by subtracting the value obtained for a window width of twelve feet (corresponding to a percentage aperture P_2) from that obtained for a window width of twenty-four feet (percentage aperture P_1). The reduction factor for one wall is calculated by adding the individual window contributions and the reduction factor for the structure is just four times that for one wall only.

A functional equation, which expresses these operations, follows.

a) Functional Equation

$$R.F. = [R_f(\omega,P_1) - R_f(\omega,P_2)][R_s(\omega,h_1) - R_s(\omega,h_2)] + R_f(\omega,P_3)[R_s(\omega,h_1) - R_s(\omega,h_2)] \quad (54)$$

$$\text{Total reduction factor} = 4\ R.F. \quad (55)$$

where P_1, P_2, and P_3 represent the percentage apertures of the wall for window widths of 24, 12, and 6 feet respectively, with the sill height at three feet and the upper level flush with the ceiling. The window sill and window top heights are respectively h_1 and h_2.

b) Determination of Parameters

The following table lists the values of the parameters utilized in the solution of the problem. The numbers in the left column refer only to subscripts. Thus P_2 = .308 and $R_f(\omega,P_2)$ = 1.65×10^{-3}. It should be noted that while in this case ω (the solid angle fraction) and E (the eccentricity) have only one value and therefore do not need to be subscripted, they are listed with subscript 1 as in many cases they can take on more than one value.

Table IV. Parameters for Example 1

	P	h	E	Figure 8 ω	Figure 7 $R_f(\omega,P)$	Figure 10 $R_s(\omega,h)$
1	0.615	3'	1.0	0.49	3.06×10^{-3}	1.0
2	0.308	6'	---	--	1.65×10^{-3}	0.90
3	0.154	-	---	--	9.1×10^{-4}	-

c) Solution

$$R.F. = (3.06 - 1.65)\times10^{-3} \cdot (1.0 - 0.90) + (9.1\times10^{-4}) \cdot (1.0 - 0.90)$$

$$= 1.41\times10^{-4} + 0.91\times10^{-4} = 2.32\times10^{-4} \text{ [one window only]}$$

$$R.F. = 9.3\times10^{-4}. \text{ Answer}$$

ii) Rectangular buildings

The contribution from windows in the wide side of rectangular buildings must be differentiated from those in the narrow side of

the structure since the eccentricity factor will be different for the two cases. The procedure employed is otherwise the same as that for square structures. An example of this follows. The plan and elevation for the structure used in this example are shown in Figure 15.

Example 2

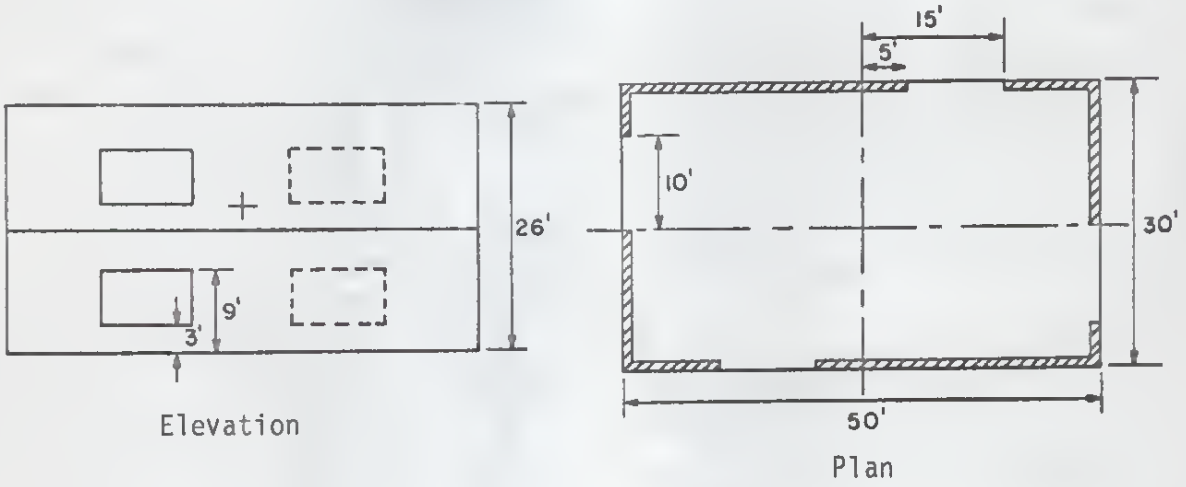

Figure 15. Structure elevation and plan for Example 2.

The reduction factor contributions from opposite walls are identical as the windows are located symmetrically. Thus it is only necessary to determine the reduction factor from two adjacent walls and multiply the answer by two. Before writing the functional equation expressing the reduction factor for this example, some clarification is necessary. P_1 and P_2 are the percentage apertures in the long side of the structure for window widths of 30 and 10 feet respectively, P_3 is the percentage aperture in the adjacent side for a window width of 20 feet.* The sill and window top heights are h_1 and h_2 and E_1 and E_2 refer to

*The percentage aperture P is always calculated for the standard window height of ten feet.

the eccentricities of the structure with apertures in the long and narrow sides respectively.

a) Functional Equation

$$\text{R.F.} = 2(\tfrac{1}{2})\, R_E(E_1)\, R_u(\omega,d)\, [R_f(\omega,P_1) - R_f(\omega,P_2)] \cdot [R_s(\omega,h_1) - R_s(\omega,h_2)]\, R_x(E_1) + 2(\tfrac{1}{2})\, R_E(E_2)\, R_u(\omega,d) \cdot R_f(\omega,P_3)\, [R_s(\omega,h_1) - R_s(\omega,h_2)]\, R_x(E_2) \qquad (56)$$

b) Determination of Parameters

Table V. Parameters for Example 2

	P	h	E	Fig. 8	Fig. 7	Fig. 10	Fig. 11	Fig. 9	Fig. 10a
				ω	$R_f(\omega,P)$	$R_s(\omega,h)$	$R_u(\omega,d)$	$R_E(E)$	$R_x(E)$
1	0.462	3'	1.667	.5620	2.80×10^{-3}	1.00	0.89	1.30	1.0
2	0.154	9'	0.60	---	1.12×10^{-3}	0.68	--	0.74	1.0
3	0.513	-	--	---	3.20×10^{-3}	--	--	--	---

In the table above, it should be noted that ω is subscripted as 1, although no subscript is needed. Furthermore, since only one ceiling height is considered (d = 26 feet), d is also subscripted as 1.

c) Solution

$$\text{R.F.} = (1.30)\,(.89)\,[2.80 - 1.12]\times10^{-3}\,[1.0 - .68] + (.74)\,(.89)\,(3.2\times10^{-3})\,[1.0 - .68] = 6.2\times10^{-4} + 6.7\times10^{-4} = 1.3\times10^{-3}.$$ Answer

d) Discussion

This example illustrates the principle of adding the responses from adjacent sides of a rectangular building. The same technique can be followed for any number of windows located in each of the walls.

2. Asymmetrically located windows.

For structures with asymmetrically located windows, the reduction factor must be calculated by adding the contributions due to each individual window. The same procedure is used if the windows have different sizes. With irregularly shaped buildings or the detector in an off-center position, the ceiling shine contribution can be evaluated by utilizing fictitious buildings (4,14).

3. Fictitious buildings (4).

A fictitious building must

i) have the same type construction as the actual building being analyzed,

ii) be symmetrical about the detector, and

iii) coincide with the ceiling being analyzed when superimposed over the actual building.

Example 3

This example illustrates the use of fictitious buildings for the ceiling shine contribution. The geometry for this example was taken from Example 7-1 in the Engineering Manual (4). With the building plan shown in Figure 16, the following must be determined:

i) the azimuthal sectors and associated decimal fractions for each section of the building that is treated separately.

ii) the fictitious buildings, indicating dimensions and walls incorporated in each. (Figure 17).

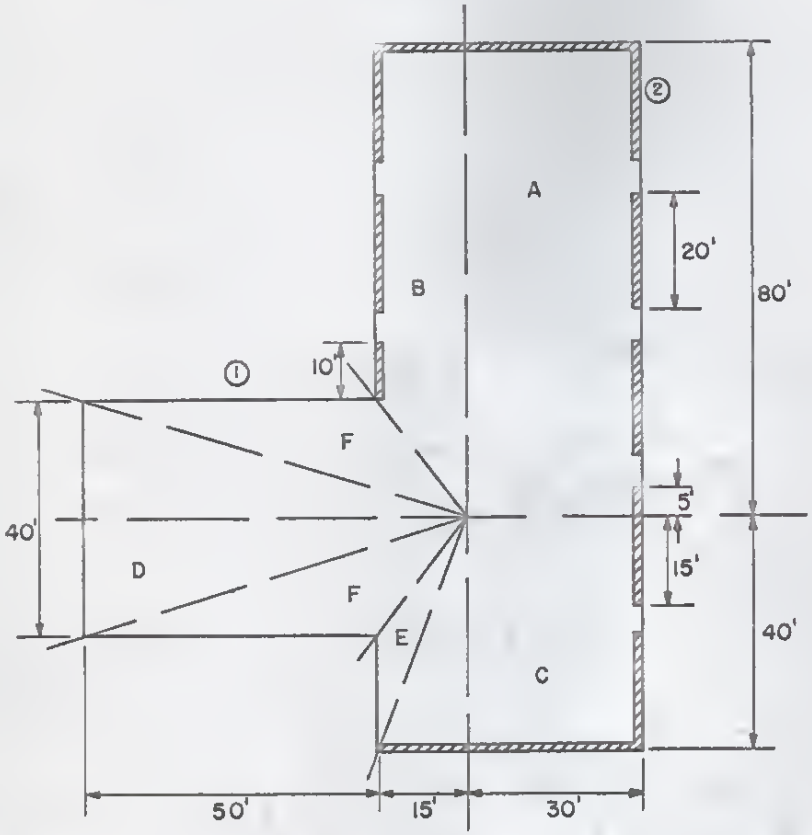

1 Glass walls - upper level 13'
sill height 3'

2 Windows - upper level 10'
sill height 5'
width 5'

Detector located 3' above the floor
One story with 13' floor height

Figure 16. Plan of structure in Example 3.

A) Determination of Azimuthal Sections

Fictitious Building	A	B	C
Azimuthal Section	$\frac{90}{360} = 0.250$	$\frac{36.9}{360} = 0.1027$	$\frac{110.6}{360} = 0.307$

D	E	F
$\frac{34.2}{360} = 0.095$	$\frac{16.3}{360} = 0.0453$	$\frac{72.0}{360} = 0.20$

Total
1.000

B) Analysis of Fictitious Buildings (Figure 17).

i) Fictitious Building A.

a) Functional Equation

$$R.F. = R_E(E)\{[R_f(\omega,P_2) - R_f(\omega,P_1) + R_f(\omega,P_4) - R_f(\omega,P_3) + R_f(\omega,P_6) - R_f(\omega,P_5)][R_s(\omega,h_1) - R_s(\omega,h_2)]\} \quad (57)$$

Here h_1 and h_2 have the usual meaning; P_1 through P_6 represent the percentage apertures determined from window widths of 10, 20, 60, 70, 110, and 120 feet respectively.

b) Determination of Parameters

Table VI. Parameters for fictitious building A

	P	h	E	Fig. 8 ω	Fig. 7 $R_f(\omega,P)$	Fig. 10 $R_s(\omega,h)$	Fig. 9 $R_E(E)$	Fig. 10a $R_x(E)$	Fig. 11 $R_u(\omega,d)$
1	0.048	5'	2.667	0.78	4.6×10^{-4}	0.89	1.70	1.0	1.0
2	0.096	10'	-	-	1.0×10^{-3}	0.48	-	-	-
3	0.288	-	-	-	2.9×10^{-3}	-	-	-	-
4	0.336	-	-	-	3.3×10^{-3}	-	-	-	-
5	0.529	-	-	-	4.8×10^{-3}	-	-	-	-
6	0.577	-	-	-	5.1×10^{-3}	-	-	-	-

c) Solution

$$R.F. = 1.70\{(1 - 0.46 + 3.3 - 2.9 + 5.1 - 4.8)\times10^{-3}\} \times \{0.89 - 0.48\} = 8.64\times10^{-4}.$$

There is no contribution from walls 3 and 4. The contribution from wall 2 is identical to that from wall 1.

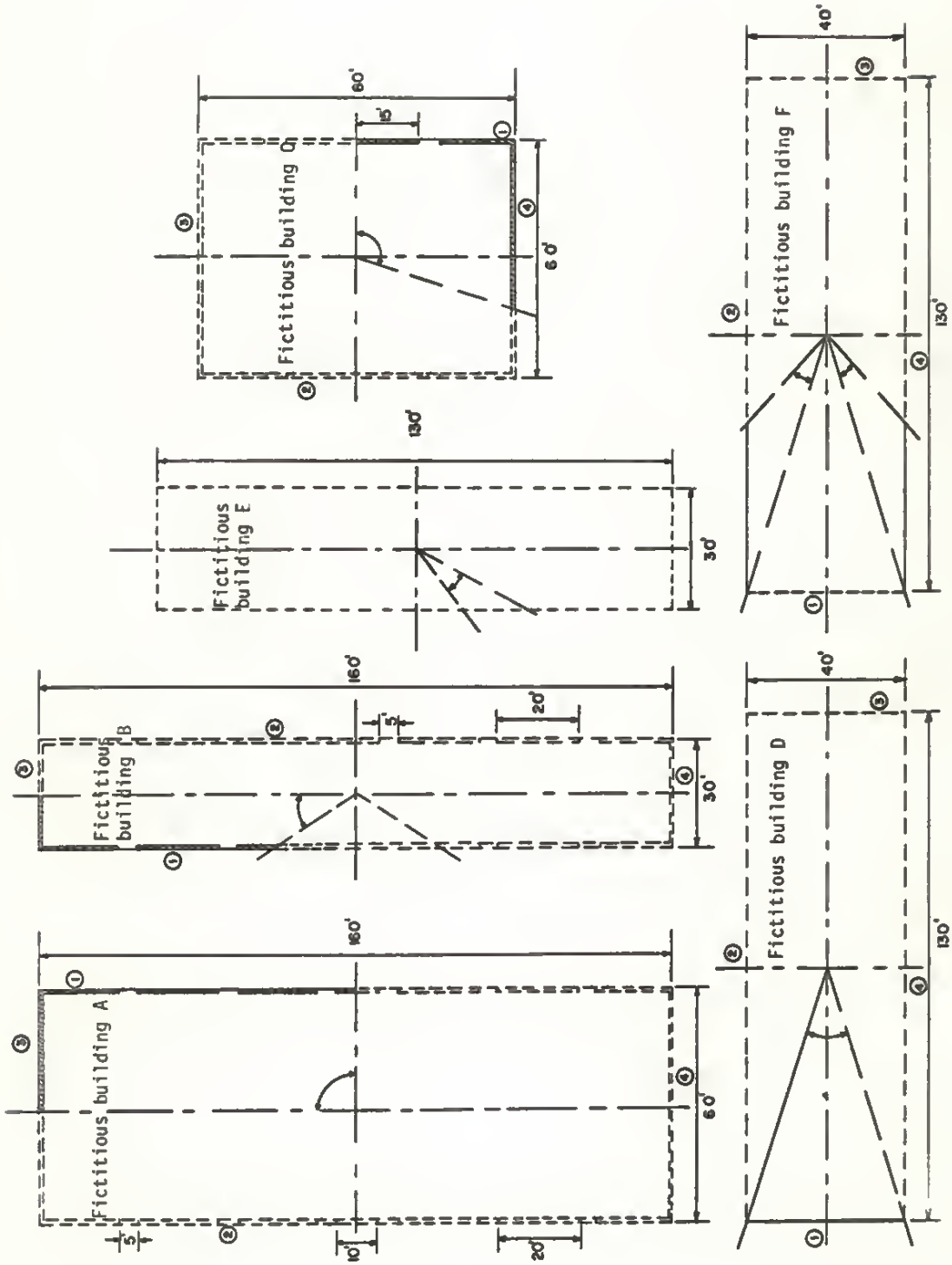

Figure 17. Plan of fictitious buildings for Example 3.

The reduction factor for fictitious building A is 1.73×10^{-3}.

Answer

ii) Fictitious Building B.

a) Functional Equation

$$R.F. = (R_E(E)\{[R_f(\omega,P_2) - R_f(\omega,P_1) + R_f(\omega,P_4) - R_f(\omega,P_3)] \times [R_s(\omega,h_1) - R_s(\omega,h_2)]\} \quad (58)$$

P_1 through P_4 represent percentage apertures obtained for window widths of 60, 70, 110 and 120 feet respectively.

b) Determination of Parameters

$R_u(\omega,d) = 1.0$. (Fig. 11)

Table VII. Parameters for fictitious building B.

	P	h	E	Fig. 8 ω	Fig. 7 $R_f(\omega,P)$	Fig. 10 $R_s(\omega,h)$	Fig. 9 $R_E(E)$	Fig. 10a $R_x(E)$
1	0.288	5'	5.33	0.62	2.1×10^{-3}	0.913	2.50	1.0
2	0.337	10'	-	-	2.4×10^{-3}	0.559	-	-
3	0.529		-	-	3.6×10^{-3}	-	-	-
4	0.577		-	-	3.9×10^{-3}	-	-	-

c) Solution

$$R.F. = (2.5)\{[2.4 - 2.1 + 3.9 - 3.6] \times 10^{-3}\}\{0.913 - 0.559\}$$

$$= 0.53 \times 10^{-3}$$

The contribution from fictitious building B is

1.06×10^{-3}. Answer

iii) Fictitious Building C.

a) Functional Equation

$$R.F. = (R_E(E))[(R_s(\omega,h_1) - R_s(\omega,h_2)][R_f(\omega,P_2) - R_f(\omega,P_1)] \quad (59)$$

P_1 and P_2 are the percentage apertures corresponding to window widths of 30 and 40 feet respectively.

b) Determination of Parameters

Table VIII. Parameters for fictitious building C.

	P	h	E	Fig. 8 ω	Fig. 7 $R_f(\omega,P)$	Fig. 10 $R_s(\omega,h)$	Fig. 9 $R_E(E)$	Fig. 10a $R_x(E)$
1	0.288	5'	1.333	0.75	2.70×10^{-3}	0.89	1.13	1.0
2	0.385	10'	-	-	3.45×10^{-3}	0.50	-	-

c) Solution

$$R.F. = (1.13)(.39)[(3.45 - 2.70)\times10^{-3}] = 3.3\times10^{-4}$$

Reduction factor from fictitious building C = 6.6×10^{-4}. Answer

iv) Fictitious Building O.

a) Functional Equation

$$R.F. = 4\, R_E(E)\, R_f(\omega,P) \quad (60)$$

b) Determination of Parameters

$\omega = 0.68$ $\quad R_E(E) = 0.50$

$E = 0.307$ $\quad P = 0.769$

$R_f(\omega,P) = 5.4\times10^{-3}$

c) Solution

R.F. = $4(0.50)5.4\text{x}10^{-3} = 1.08\text{x}10^{-2}$

Reduction factor from building D = $1.08\text{x}10^{-2}$. Answer

v) Fictitious Building E.

a) Functional Equation

$$\text{R.F.} = 4\, R_E(E)\, R_f(\omega,P) \tag{61}$$

b) Determination of Parameters

$\omega = 0.62$ $R_E(E) = 2.26$ $R_f(\omega,P) = 4.8\text{x}10^{-3}$

c) Solution

R.F. = $4(2.26)(4.8\text{x}10^{-3}) = 4.33\text{x}10^{-2}$.

Reduction factor from building E = $4.33\text{x}10^{-2}$. Answer

vi) Fictitious Building F.

a) Functional Equation

$$\text{R.F.} = 4\, R_E(E)\, R_f(\omega,P) \tag{62}$$

b) Determination of Parameters

$E = 3.25$ $R_E(E) = 1.9$ $\omega = 0.68$ $R_f(\omega,P) = 5.4 \times 10^{-3}$

c) Solution

R.F. = $4(1.9)(5.4\text{x}10^{-3}) = 4.1\text{x}10^{-2}$

Reduction factor from building F = R.F. = $4.1\text{x}10^{-2}$. Answer

C) Total Reduction Factor for Building in Figure 16.

R.F. = $0.250(1.73\text{x}10^{-3}) + 0.1027(1.06\text{x}10^{-3})$

$+ 0.307(6.6\text{x}10^{-4}) + 0.095(1.08\text{x}10^{-2}) + 0.0453(4.33\text{x}10^{-2})$

$+ 0.20(4.1\text{x}10^{-2}) = 1.19\text{x}10^{-2} = 0.012$. Answer

D) Discussion

The total reduction factor in a complex structure is equal to the sum of the reduction factors for each fictitious building employed, multiplied by the respective azimuthal sectors.

3.1.3 Accuracy of the Design Curves

Several errors are introduced in the calculation of the reduction factor inside a multistory building. There are errors associated with the use of the Chilton-Huddleston formula (5 to 10%, reference 8); errors in simulating a fallout field with a cobalt-60 field (5%, Appendix C), inaccuracies involved in the values for the dose angular distribution of radiation (10 to 15%) and uncertainties introduced by the particular choice of the build-up factor (7). Spencer has estimated the possible error of the integrated dose angular distribution curve to be 8%.* Difficulties in reading the dose angular distribution curve in reference 1 would raise the 8% to 10-15%, assuming the 8% estimate for the integrated dose angular distribution curve applies to the dose angular distribution curve. The uncertainty in the build-up factor will not result in a significant deviation, because of the small value of the build-up factor per se in these calculations.

These errors appear in every calculation of the reduction factor and should be combined with the uncertainty resulting from the use of numerical Gaussian quadrature in the integration of Eq. (31) to obtain a total error. To this error, common to each of the design curves, must be added the uncer-

---

* LeDoux, J. C., "Various Sources of Uncertainties in Fallout Shielding Methods of Analysis" (unpublished).

tainty introduced by the averaging processes and plotting techniques utilized in developing such design curves.

To determine the error resulting from the use of Gaussian integration, several different order quadratures were employed in the solution of Eq. (31). The reduction factors thus obtained were plotted versus the order of quadrature employed. For even order quadratures, an asymptotic increase in the value of the reduction factor was obtained for orders greater than six. The difference between the apparent asymptotic value and that of an even order Gaussian quadrature of six (or greater) was less than one per cent.

Figure 7 is accurate within the error involved in all design curves as examined above, which is estimated from the above standard deviations to be approximately fourteen per cent. The uncertainty introduced by the averaging processes in Figure 9 varies from three to about thirty-four per cent. Thus the accuracy of the eccentricity factor ranges from fourteen per cent to forty-two per cent. The accuracy is best for eccentricities less than and close to 1.0, and becomes progressively poorer as the eccentricity becomes much larger than 1.0.

The error associated with Figure 10 varies from fourteen per cent to about thirty-three per cent, the error increasing with increasing solid angle. The same general considerations hold true for Figure 11; that is, the accuracy of this figure decreased as the solid angle is increased. In addition the accuracy decreases at greater distances from the source plane. This latter characteristic is because of larger errors in the values used for the dose angular distribution of radiation.

3.1.4 Comparison With Other Ceiling Shine Measurements

A comparison is made in Figure 18 among the reduction factors obtained through use of the current model and two other techniques. The ceiling shine contribution obtained through the use of Eisenhauer's technique (15) could only be directly plotted for a roof approaching infinite size. The method of Batter and Velletri (16) is based on a semianalytical formula derived from measurements of scattering of radiation from point sources off concrete and steel slabs. This formula could not be applied to the infinite ceiling case. The model developed in this work yields the reduction factor in any concrete structure as a function of building dimensions, aperture sizes and locations, and detector locations.

According to Figure 18, Batter and Velletri's method appears to underestimate the ceiling shine contribution while Eisenhauer's technique overestimates it for the only comparison which can be made.

3.2 Discussion and Conclusions

The set of charts developed in this study have been obtained for detector locations three feet above the floors of a multistory structure whose floor to ceiling distance is thirteen feet; thus, although they can be used in almost any case, strictly accurate answers can be obtained only for structures meeting these specifications. The reliability of the curves decreases as the floor to ceiling distance deviates more and more from thirteen feet. Since, however, for actual cases reasonable deviations will be at most a few feet, the accuracy of the charts is not greatly affected for aboveground stories. In the case of an exposed basement, however, the portion exposed

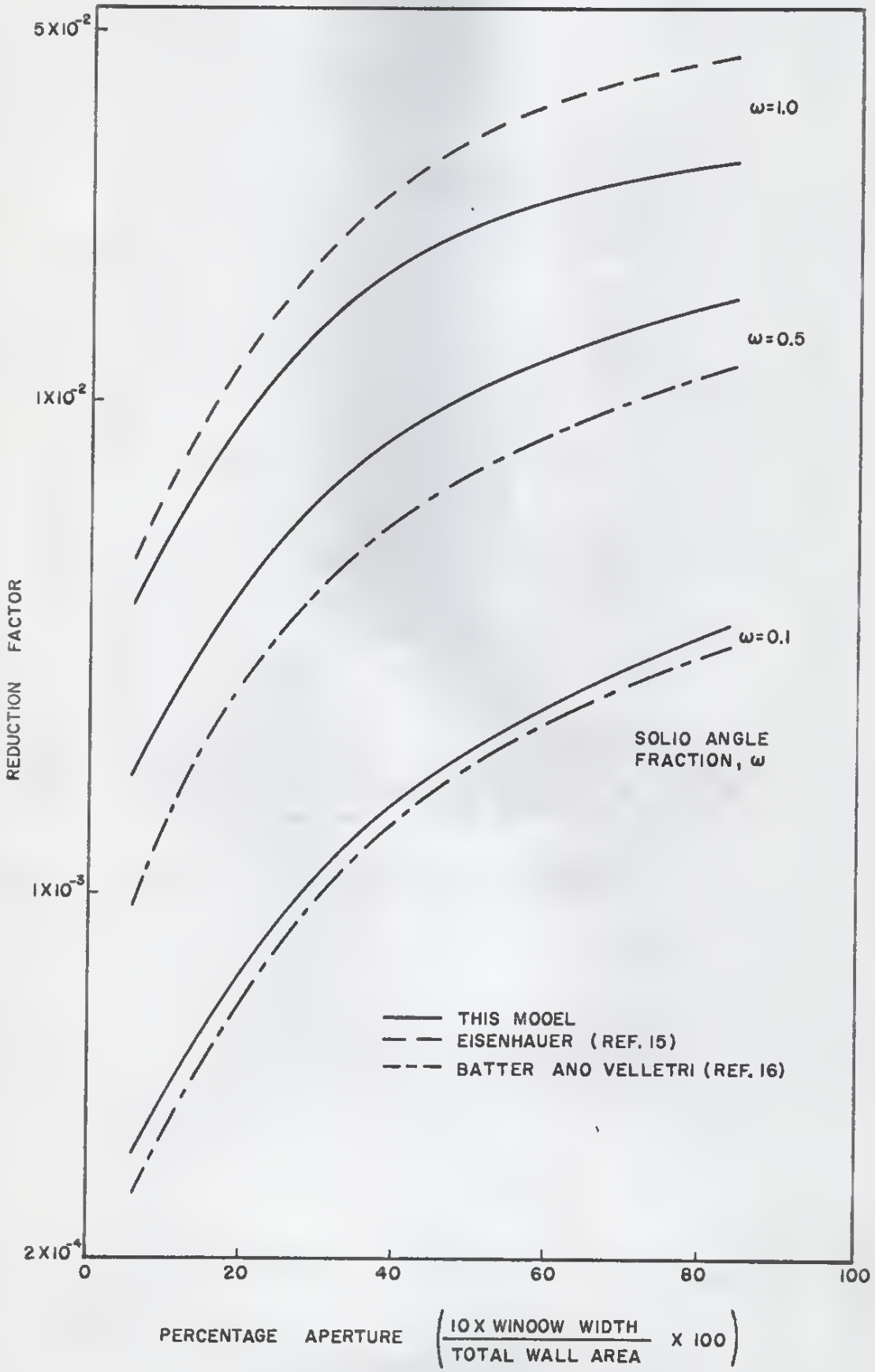

Figure 18. Comparison of ceiling shine reduction factors.

to direct radiation would be treated by the curves as the first floor of a building, thus the deviation from thirteen feet would be very great and the charts could at best provide only an estimate of the correct reduction factor.

There is also another factor, inherent in the initial assumptions of the model used, which affects the accuracy of the design curves. In the theory the walls of the structure are presumed to have zero linear thickness. In actuality the walls will have a finite thickness so that it will be physically possible for the incident radiation to penetrate through the edges of the window and contribute to the ceiling shine dose rate. Thus, if the physical dimensions of the window are used the charts will yield a non-conservative answer, as they would fail to take into account the lip penetration through the window edges. To obtain a more realistic answer from the charts, one should determine an effective window size (i.e., the physical dimensions of the window are enlarged to account for lip penetration).

The statistical deviations associated with the charts appear to be rather large. The accuracy of all charts would be improved by use of more recent values for the dose angular distribution of fallout radiation at various heights and a more exact formula for the dose rate albedo. Unfortunately some compromise had to be reached in the development of the curves themselves. The sill-height and ceiling-height correction factors depend not only on the solid angle subtended by the ceiling at the detector, but also, to a lesser extent, on the eccentricity of the structure and the percentage aperture of the window. The substantially large deviations associated with the development of these charts are solely due to the averaging processes that had to be employed in order that all charts could be presented in a relatively easy form.

3.3 Further Investigations

The problem of ceiling shine radiation, as studied in this monograph, has been restricted to the analysis of radiation which enters through a window and scatters off the ceiling of the structure. There is, however, one other aspect of the ceiling shine problem which offers excellent opportunity for further investigation.

The model, presented in this study, can be extended to cases in which radiation is first downscattered and then enters an aperture. One such problem, for instance, is afforded by the case of a structure with roof overhang and a high band of windows. This problem can be further extended to determine the amount of overhang needed to minimize the simultaneous effects of ceiling shine and skyshine.

A study should also be made of the effect of interior partitions on the reduction factor due to ceiling shine radiation alone, and also of the effect of a floor barrier placed between the ceiling and the detector.

The set of curves presented in this report is developed for a structure exposed to an infinite field of fallout radiation. In many instances this is not the case, as the fallout will lie in a strip around the building in question. Thus an identical study should be conducted for limited strips of contamination and a comparison be made with the results achieved with the infinite field of fallout radiation. This study will require a knowledge of the dose angular distribution of radiation at various heights above different limited strips of contamination.

Finally the set of curves should be extended to include cases in which the first floor ceiling is at a height different from thirteen feet, i.e., the case of a partially exposed basement.

4.0 ACKNOWLEDGEMENT

The author wishes to express his gratitude to Dr. R. E. Faw and Dr. W. R. Kimel, Head of the Kansas State University Department of Nuclear Engineering, under whose direction this work has been accomplished. Sincere appreciation is also extended to Mr. J. A. Baran for his continuous help in several phases of this study, and to the staff of the Argonne National Laboratory Computing Center for their assistance in the use of the CDC-3600 digital computer.

5.D LITERATURE CITED

1. J. A. Baran, "Blockhouse Dosage Contributions Resulting from Window-Collimated Ceiling-Scattered Fallout Radiation", Kansas State Engineering Experiment Station Special Report Number 32, 1963.

2. L. V. Spencer, "Structure Shielding Against Fallout Radiation from Nuclear Weapons", NBS Monograph 42, June 1, 1962.

3. Clarke, E. T. and Buchanan, J. O., "Radiation Shielding Against Fallout", Nucleonics, 20, No. 8, pp. 143-6 (1962).

4. Eisenhauer, C. M., "Design and Review of Structures for Protection from Fallout Gamma Radiation", PM-100-1, Department of Defense, Interim Edition, February, 1965.

5. Fallout Shelter Surveys: Guide for Architects and Engineers. Office of Civil Defense and Defense Mobilization, National Plan Appendix Series, NP-1D-2, December, 1961.

6. J. C. LeDoux, et al., Shelter Design And Analysis, Vol. II, TR-20, Office of Civil Defense, May, 1964.

7. Chilton, A. B., Holoviak, D., and Donovan, L. K., "Determination of Parameters in an Empirical Function for Build-up Factors for Various Photon Energies", U. S. Naval Civil Engineering Laboratory Technical Note N-389, August, 1960.

8. Fu, C. Y. and Chilton, A. B., "Exposure from a Point Isotropic Source Located at the Surface of a Thick Concrete Slab", University of Illinois Report NRSS-2, July, 1966.

9. Chilton, A. B. and Huddleston, C. M., "A Semiempirical Formula for Differential Dose Albedo for Gamma Rays on Concrete", U. S. Naval Civil Engineering Laboratory, Technical Report R 228, November 16, 1962.

10. Chilton, A. B., Davisson, C. M., Beach, L. A., "Parameters for C-H Albedo Formula for Gamma Rays Reflected from Water, Concrete, Iron, and Lead", Trans. Am. Nuc. Soc., 6, 2, p. 656 (1965).

11. Jones, T. H., et al., "Experimental Determination of the Gamma Ray Angular Dose Albedos of Concrete, Aluminum, and Steel", USNRDL-TR-790, October 6, 1964.

12. Nielsen, K. L., Methods in Numerical Analysis, Second Edition, McMillan Co., 1964.

13. Handbook of Mathematical Functions, AMS-55, National Bureau of Standards, Department of Commerce, p. 916, June, 1964.

14. Shelter Design and Analysis, Vol. I, TR-2D, Office of Civil Defense, May, 1964.

15. Eisenhauer, C. M., "An Engineering Method for Calculating Protection Afforded by Structures Against Fallout Radiation, NBS-781D, February, 1963.

16. Batter, J. F. and Velletri, J. D., "The Effects of Radiation Reflected from the Ceiling on the Dose Rate Within Structures", TO-B 63-25, April, 1963.

17. The Effects of Nuclear Weapons, S. Glasstone, Editor (U. S. Government Printing Office, 1962).

18. C. S. Cook, "Energy Spectrum of Gamma Radiation from Fallout", USNRDL-TR-318, October, 1959.

19. A. T. Nelms and J. W. Cooper, "U-235 Fission Product Decay Spectra at Various Times After Fission", Health Physics, 1, 427 (1959).

20. Carl Miller, "Biological and Radiological Effects of Fallout from Nuclear Explosions", Office of Civil Defense, TR-38, June, 1966.

21. Kimel, W. R., et al., "Scattering of Fallout Radiation from Ceilings of Protective Structures", Kansas State University Engineering Experiment Station Special Report No. 72, 1966.

22. Fano, U., Spencer, L. V., and Berger, M. J., "Penetration and Diffusion of X-Rays", Handbuch der Physik, 38 II, 66D (Springer-Verlag, Berlin, Germany, 1959).

23. Faw, R. E., "Notes on Structure Shielding Against Fallout Radiation", Special Report Number 63, Kansas State University Engineering Experiment Station, December, 1965.

24. Raso, D. J., "Monte-Carlo Calculations on the Reflection and Transmission of Scattered Gamma Radiations", Tech. Dps. Inc. Report No. TD-B 61-39, May, 1962.

6.0 APPENDICES

APPENDIX A

Fallout Spectra and Characteristics

Radioactive fallout is observed whenever a nuclear weapon is exploded. The concentration of fallout in the vicinity of the point of detonation (ground zero) is dependent on the distance above (or below) the surface of the earth at which the detonation occurs, and upon the yield of the weapon. The spectral characteristics of fallout radiation, however, do not appear to be strongly dependent on weapon yield, type, or conditions of detonation (17).

Fallout is usually classified into local and world-wide. World-wide fallout normally results only from large explosive yields. It is composed of very small particles which are dispersed in the stratosphere. Because of the long delay period before deposition, only the relatively long-lived nuclides such as Sr-90 and Cs-137 remain as radioactive nuclides. The wide distribution over the world results in only light deposits of the world-wide fallout compared to the deposit density possible for local fallout.

The exact distribution of radioactive fallout is dependent on the metereological conditions at the time of burst and shortly thereafter. Quite naturally the dose received from fallout radiation will be related to the fallout distribution at different times after the explosion. Figure 19 illustrates the total fallout exposure from a large explosion, indicating how the fallout was carried by the winds from the point of detonation. It is clear from the figure that intense fallout can occur in areas far beyond blast and heat effects associated with the explosion. This makes it reasonable to consider fallout as a problem separate from blast and heat complications.

When the detonation takes place near the earth's surface, large quantities of debris are sucked up in the fireball. This debris mixes intimately with the

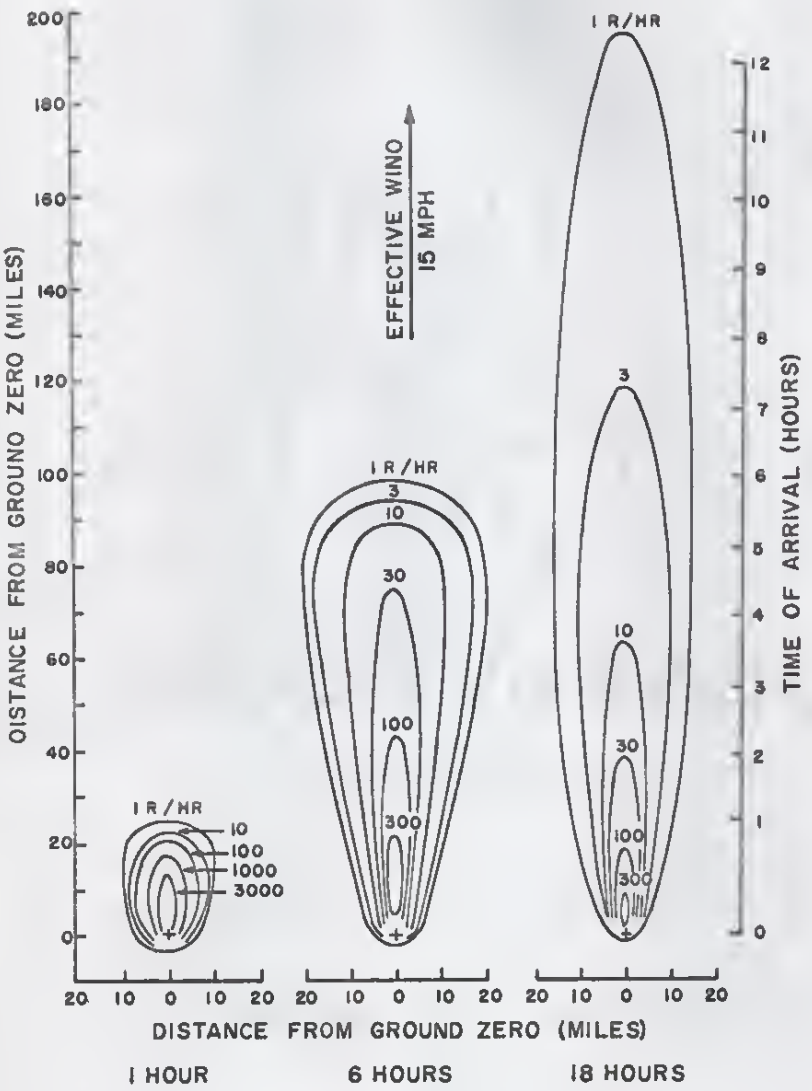

Dose rate contours from early fallout at 1, 6, and 18 hours after a surface burst with 1 megaton fission yield (15 mph effective wind speed). (17)

Figure 19. Dose rate contours from fallout.

radioactive products yielded by the weapon, and upon cooling settles to the earth's surface, bringing much of the radioactivity back to earth within a few miles of ground zero. If the burst is at high altitude, however, the debris is absent, and the radioactive products of the weapon form the fallout. These products are in the form of an exceedingly fine aerosol, due to the extremely high temperatures, and can be carried by the winds for many hundreds of miles before diffusing down to the earth's surface. Thus for a sufficiently high burst, the only residual radioactivity observed near ground zero is that induced in the soil by activation by the neutrons from the weapon. In most soils the most significant gamma-ray emitting radioisotopes are Na-24, Al-28, and Mn-56.

Fallout, therefore, consists of the fission products and whatever isotopes are produced by neutron activation of the materials in the immediate environment of the explosion. One such neutron-induced radioactivity occurs because of the presence of U-238 in nuclear weapons. The $U^{238}(n,\gamma)U^{239}$ reaction produces U^{239} which decays to Np^{239} by beta emission with a half-life of 23.5 minutes. Because of the relatively short half-life and the low energy of the emitted gammas (73 Kev), the radiation of U^{239} is of importance only in the early stages after detonation, and its contribution to the spectral characteristics of fallout at later times can be altogether neglected (18). Np^{239}, however, decays with a half-life of 2.3 days, and the photons emitted have energies of 106, 223, and 278 Kev, so that it is possible for the radiation from Np^{239} to contribute to the low energy portion of the spectrum (18).

The fallout radiation energy spectrum changes with time. This feature comes about because of the different decay rates of the many radionuclides present in the fallout. Since each nuclide decays at its own rate, a different

spectrum can be considered in existence at different times. Examples of fission spectra at successive times are given in reference 19.

Because of the time variation of the gamma-ray fission spectrum, it has been necessary to make some decision regarding the choice of a spectrum to be utilized in this study.

Nelms and Cooper (19) have made two types of tabulation of gamma radiation energy spectra from U^{235} prompt fission products as functions of time. In one tabulation the radiations from all radioactive fission product nuclides are included, and in the other, radiations from selected volatile fission products have been removed. The values listed in those tables, being for fission-product activity only, neglect the contribution of Np^{239} to the fallout spectrum.

The energy spectrum from fission at 1.12 hours, with the volatile components removed, was chosen for three reasons: a) the spectrum at this time is representative of the spectra at earlier times, and most of the exposure to radiation is apt to occur during the first few hours, b) volatile fission products would to a large extent remain separated from the fallout material, and c) the penetration properties of fallout are, except for very large penetrations, not very sensitive to spectral changes (2).

The choice of the 1.12 hours spectrum leaves open the possibility of three sources of uncertainty: a) the contribution at low energies of the Np^{239} photons is neglected, b) the removal of the volatile components seems to depend on the half-life of the gaseous material (longer half-life materials have larger percentage of removal than shorter lived ones), and c) the energy spectrum does depend not only on time but also on the variation in distance from ground zero and the particle size, which affect the "fractionation" number (20).

Neither of the first two errors appears to be too critical. The contribution of the lower energy portion of the spectrum to the total dose from fallout radiation is less than five tenths of one percent, and the half-lives of the volatile components removed by Nelms and Cooper, Br, Ru, Kr, I, and Xe, are long enough to warrant the assumption that the percentage of removal be one hundred percent.

The third error is caused by the fact that there is such a large range in the thermal stability of the condensates of the fission product nuclides that the normal abundance ratios of the fission nuclides in fallout are changed. Any alteration in the abundance ratios of the fission products relative to the original fission yield abundances ratios is called fractionation (20). Fractionation varies depending on the size of the particles and, as the different size particles have different deposition times, fractionation will vary as the distance (and time) from the location of the explosion is varied.

In large fallout particles (short deposition times) the relative concentration of volatile radionuclides is low and that of the more refractory radionuclides is high. Thus for relatively short times following the nuclear event, the concentration of the volatile components is low and the chosen spectrum is a good approximation of the fallout spectrum. As the time from the explosion is increased, however, smaller particles will begin to settle, which will be relatively rich of volatile nuclides, thus the assumed spectrum is not a satisfactory approximation.

Table 9 was obtained from the values listed in reference 19 by multiplying the yield at each energy by the width of the respective energy group.

Table IX. Energy content of gamma rays from prompt fission of U-235 (volatile components removed)

Group	Energy (Mev)	Fraction of Total Energy Content of Spectrum
1	0.2128	0.0062922
2	0.2554	0.0015466
3	0.3194	0.0324561
4	0.4257	0.0413492
5	0.5108	0.0110158
6	0.6386	0.1065483
7	0.8514	0.0941630
8	1.0217	0.1053941
9	1.2772	0.1059866
10	1.7029	0.2684871
11	2.0435	0.0511426
12	2.5545	0.1706286
13	3.4059	0.0049896

APPENDIX B

Gaussian Quadrature Accuracy in Quadruple Integration of the Ceiling Shine Equation

The complexity of the required integrations in this thesis made it necessary to fit the data with an empirical expression and then use formal analytical methods. This technique is commonly known as numerical integration. The method of numerical integration used in this study is called Gaussian Quadrature. This procedure notes the values of the ordinate y at n predetermined values of x. The sum of the products of the ordinate y, multiplied by a predetermined constant, is multiplied by the difference in the integration limits of x to yield the desired integral.

Suppose that

$$I = \int_a^b f(x)dx \tag{63}$$

where f(x) is a known function but whose integral is not easily evaluated. The principle of the Gaussian Quadrature is to obtain the best subdivision of the interval (a,b), the value of f(x) at these points, and the coefficients to multiply the functional value to yield the desired integral (12).

First the limits of integration must be transformed from (a,b) to (-1,1). This is accomplished by letting

$$x = \frac{1}{2}(b-a)u + \frac{1}{2}(a+b) \tag{64}$$

so that

$$f(x) = f[\frac{1}{2}(b-a)u + \frac{1}{2}(b+a)] = v(u) \tag{65}$$

and $$dx = \frac{1}{2}(b-a)du \tag{66}$$

and the integral becomes

$$\int_a^b f(x)dx = \frac{1}{2}(b-a)\int_{-1}^{1} v(u)du \tag{67}$$

We then state that

$$\int_{-1}^{1} v(u)du = w_1 v(u_1) + w_2 v(u_2) + w_3 v(u_3) + \ldots + w_n v(u_n) \tag{68}$$

In this fashion, utilizing n predetermined values of x, a polynomial of (2n-1) degree would be exactly fitted.

The u_i are the points of subdivision of the interval (-1,1), and are chosen to be the zeroes of the Legendre polynomials of order n. These zeroes are known and tabulated, and then the corresponding values of w_i can be evaluated (Christoffel numbers). Table X lists values of u_i and w_i for different values of n (order of quadrature). Since $u_i = -u_{n-i+1}$ and $w_i = w_{n-i+1}$, only half of the values are tabulated (13).

Table X. Roots and weights for Gaussian quadrature.*

n	i	u_i	w_i
3	1	0.0000000000	0.8888888889
	2	0.7745966692	0.5555555556
4	1	0.3399810436	0.6521451549
	2	0.8611363116	0.3478548451

* This table is reproduced directly from reference 13.

Table X (continued)

n	i	u_i	w_i
5	1	0.0000000000	0.5688888889
	2	0.5384693101	0.4786286705
	3	0.9061798459	0.2369268850
6	1	0.2386191861	0.4679139345
	2	0.6612093865	0.3607615730
	3	0.9324695142	0.1713244924
7	1	0.0000000000	0.4179591837
	2	0.4058451514	0.3818300505
	3	0.7415311856	0.2797053915
	4	0.9491079123	0.1294849662
8	1	0.1834346425	0.3626837834
	2	0.5255324099	0.3137066459
	3	0.7966664774	0.2223810344
	4	0.9602898565	0.1012285363
9	1	0.0000000000	0.3302393550
	2	0.3242534234	0.3123470770
	3	0.6133714327	0.2606106964
	4	0.8360311073	0.1806481607
	5	0.9681602395	0.0812743884
10	1	0.1488743390	0.2955242247
	2	0.4333953941	0.2692667193
	3	0.6794095683	0.2190863625
	4	0.8650633667	0.1494513491
	5	0.9739065285	0.0666713443
15	1	0.0000000000	0.2025782419
	2	0.2011940940	0.1984314853
	3	0.3941513471	0.1861610000
	4	0.5709721726	0.1662692058
	5	0.7244177314	0.1395706779
	6	0.8482065834	0.1071592205
	7	0.9372733924	0.0703660475
	8	0.9879925180	0.0307532420
20	1	0.0765265211	0.1527533871
	2	0.2277858511	0.1491729864
	3	0.3737060887	0.1420961093
	4	0.5108670019	0.1316886384
	5	0.6360536807	0.1181945320

Table X (continued)

n	i	u_i	w_i
20	6	0.7463319065	0.1019301198
	7	0.8391169718	0.0832767416
	8	0.9122344282	0.0626720483
	9	0.9639719273	0.0406014298
	10	0.9931285992	0.0176140071

It is difficult to determine accurately the magnitude of the error associated with the use of different order quadratures. A test is performed to determine the accuracy of the quadruple integration involved in this thesis.

First the accuracy of the θ and ϕ integrations is determined by calculations of the reduction factor at a position three feet above the source plane in the center of a structure of dimensions 19 x 19 x 8.17', with a centrally located window covering approximately 4.6% of one wall (21). (The dimensions of this particular problem is so chosen because they represent the physical dimensions of the blockhouse at the Kansas State University Nuclear Engineering Shielding Facility.) In these calculations the order of the Gaussian quadratures in the x and y integrations is held constant, while the order of the quadratures for the integrations over the incident polar and azimuthal angles is increased for each successive calculation. The results are tabulated in Table XIa.

Table XIa. Reduction factor in square blockhouse (19 x 19 x 8.17'), three feet above the source plane-4.6% aperture (θ, ϕ Integration-x,y fixed).

Gaussian Quadrature Order				Reduction Factor
x	y	θ	ϕ	
3	6	3	3	0.00017489
3	6	4	4	0.00017494
3	6	5	5	0.00017495
3	6	6	6	0.00017495

Inspection of these values shows that an order three in the θ and ϕ integrations is adequate. Increasing the quadrature order would increase the accuracy by less than 0.04%. Thus a Gaussian quadrature of order three accurately simulates the integration.

Having determined the accuracy of the angular integrations, the integrand of the x and y integrations of Eq. (31) (θ and ϕ integrations are performed with a quadrature of order three) is evaluated and plotted in Figure 20. The volume contained by the surface represents the true value of the reduction factor. This volume, however, cannot be determined accurately so that other means must be employed to ascertain the true value of the reduction factor.

To this end different order quadratures in the x and y integrations are again used to determine the reduction factor at the central point three feet above the floor (0',9,5',5.17') in the structure. Table XIb. lists the values obtained for each quadrature.

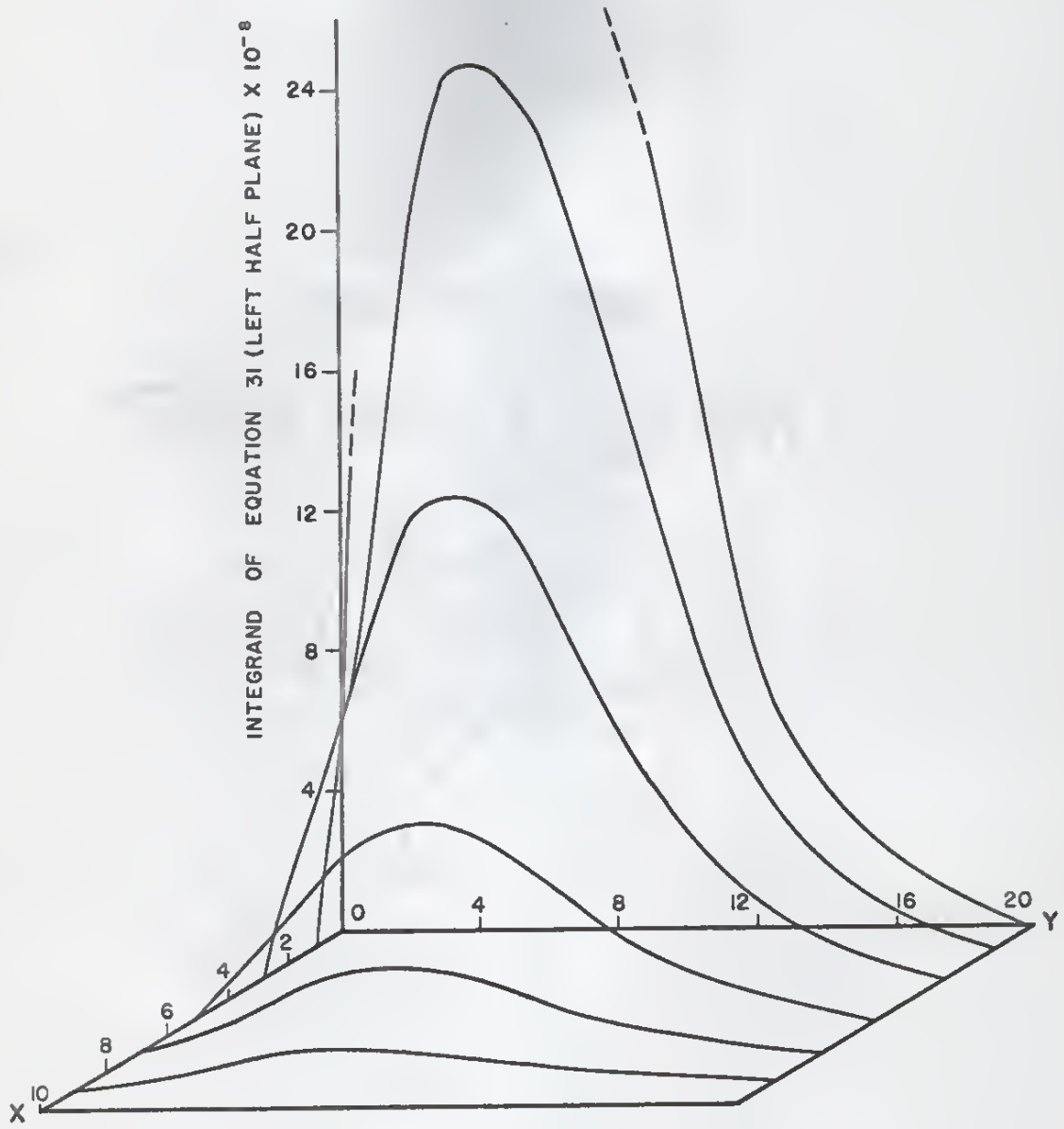

Figure 20. Graphical representation of integrand of Eq. (31).

Table XIb. Reduction factor in square blockhouse (19 x 19 x 8.17'), three feet above the source plane-4.6% aperture (x, y Integration-θ,φ fixed).

Gaussian Quadrature Order				Reduction Factor
x	y	θ	φ	
3	4	3	3	0.00017457
3	5	3	3	0.00019464
3	6	3	3	0.00017489
3	7	3	3	0.00018893
4	8	3	3	0.00017371
4	9	3	3	0.00018497
5	10	3	3	0.00017408
7	15	3	3	0.00018013
10	20	3	3	0.00017406

Figure 21 is a plot of the value of the reduction factor versus the order of the quadrature employed. This figure is obtained for a window of dimensions 3 feet wide by 2.34 feet high, located centrally with respect to the x-axis, and with the sill at a distance four feet above the source plane. Symmetry with respect to the x = 0 axis is employed. One can see that even order quadratures yield values oscillating around a value of 1.740×10^{-4}, while odd order values are constantly decreasing with increasing order of quadrature. A value of 1.741×10^{-4} can be obtained from Figure 21 as the best estimate of the true value of the reduction factor for this configuration.

An analysis of Figure 21 can furnish some interesting information.

a) Odd order quadratures yield answers which are conservative.

b) The true value of the reduction factor lies close to the solutions obtained by even order quadratures, but these orders yield values which are not conservative.

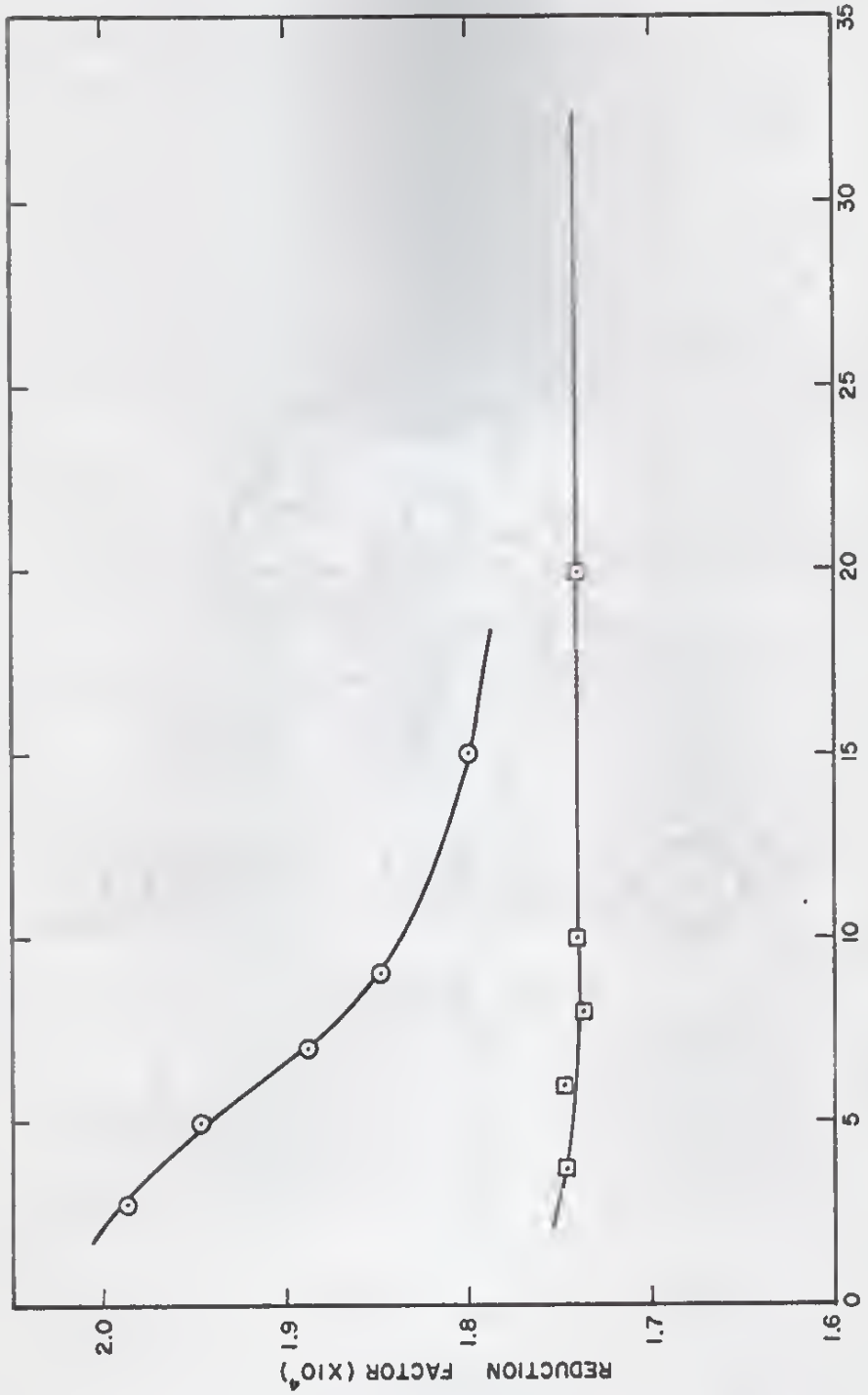

Figure 21. Reduction factor as a function of the order of Gaussian quadrature utilized in the integration in the computer codes.

c) The error associated with the use of even order Gaussian quadrature of order six in the y integration and order three in the x integration, instead of larger orders, is less than one per cent. Because of this last characteristic, this particular order has been chosen for the x and y integrations in this thesis.

APPENDIX C

Accuracy of Simulating an Infinite Field of Fallout Radiation by an Infinite Plane Isotropic Source of Cobalt-60 Radiation

Ideally, all calculations for the design curves should have been performed utilizing the energy spectrum for fallout radiation, shown in Figure 1. This, however, would have required an inordinate amount of computer time. Thus it was decided to analyze several situations making use of the spectrum and to compare them with results obtained for identical situations with an infinite field of cobalt-60 radiation. Such comparison establishes a criterion for correcting the cobalt-60 results. Use of the discrete fission spectrum for design calculations requires a knowledge of the dose angular distribution of radiation at the height of the ceiling under consideration for each of the discrete energies of the spectrum. Although the dose angular distribution for the 1.12 hour fallout spectrum is given by Spencer (2), equivalent curves are not presented for each separate energy. Ordinarily, such distributions are calculated by the moments method (22). This involved and lengthy method was discarded in favor of a somewhat less accurate, but much shorter approximate solution.

Consider an infinite field of fallout radiation as an infinite plane isotropic source of gamma radiation (23). Let $D_u(r)$ be the unscattered dose rate at a distance r from a point isotropic source (23). The differential unscattered dose rate from area dA shown in Figure 22 is given by

$$dD_u = \frac{e^{-\mu(E_0)r}\,\mu_a(E_0)E_0}{4\pi r^2 \alpha}\,\rho d\rho d\phi_0 \qquad (69)$$

where E_o is the energy of the incident radiation,

$\mu(E_o)$ is the total linear gamma ray attenuation coefficient for the medium,

$\mu_a(E_o)$ is the linear gamma ray energy absorption coefficient for the medium, and

α is a constant necessary to convert the units of the expression to milliroentgens per hour.

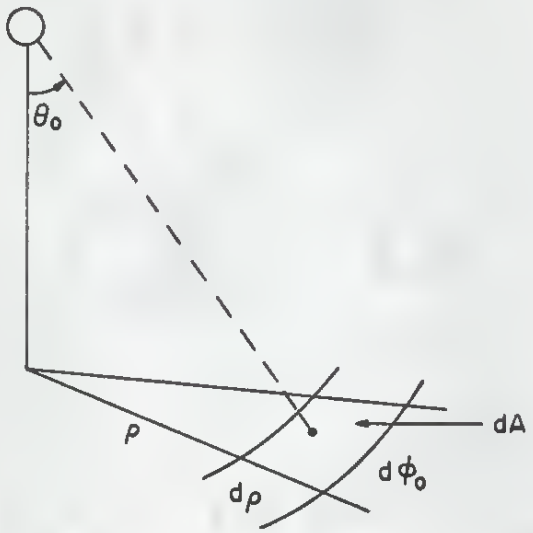

Figure 22. Plane-detector geometry.

Utilizing trigonometric relations, the equation above can be rewritten as

$$dD_u = \frac{e^{-\mu(E_o)d/\cos\theta_o}}{4\pi\alpha\cos\theta_o}\,\mu_a(E_o)E_o\,d\phi_o d(\cos\theta_o). \tag{70}$$

An integration is then performed over the azimuthal and polar angles.

$$D_u = \int_0^1 \frac{e^{-\mu(E_o)d/\cos\theta_o}}{2\alpha\cos\theta_o}\,\mu_a(E_o)E_o\,d(\cos\theta_o) \tag{71}$$

The total dose rate will be the product of the unscattered dose rate times the proper build-up factor.

$$D = \int_0^1 \frac{B(\mu d/\cos\theta_0)\ e^{-\mu(E_o)d/\cos\theta_0}}{2\alpha\cos\theta_0}\ \mu_a(E_o)E_o\ d(\cos\theta_0) \qquad (72)$$

The unscattered and total dose rates at any height must be normalized to the total dose rate at three feet above the source plane so that results may be compared with dose rates obtained by Spencer (2). The dose rate three feet above the source plane is given by

$$D_o = \frac{1}{2}\frac{\mu_a(E_o)E_o}{\alpha}\int_0^1 \frac{B[\mu(E_o)3'/\cos\theta_0]\ e^{-\mu(E_o)3'/\cos\theta_0}}{\cos\theta_0}\ d(\cos\theta_0) = \frac{1}{2}\frac{\mu_a(E_o)E_o\kappa}{\alpha} \qquad (73)$$

where κ is a constant determined through evaluation of the integral in Eq. (73). The build-up factor equation used is again of the form

$$B(\mu\rho) = 1 + a'\mu(E_o)\rho\ e^{b\mu(E_o)\rho} \qquad (10)$$

where a' and b are parameters dependent on the energy of the radiation and the composition of the medium.

From Eqs. (71), (72) and (73),

$$\frac{D_u}{D_o} = \int_0^1 \frac{e^{-\mu d/\cos\theta_0}}{\kappa\cos\theta_0}\ d(\cos\theta_0), \qquad (74)$$

and

$$\frac{D}{D_o} = \int_0^1 \frac{B(\mu d/\cos\theta_0)\ e^{-\mu d/\cos\theta_0}}{\kappa\cos\theta_0}\ d(\cos\theta_0), \qquad (75)$$

where, as defined by Eq. (73),

$$\kappa = \int_0^1 \frac{B(\mu(E_o)3'/\cos\theta_o)\ e^{-\mu(E_o)3'/\cos\theta_o}}{\cos\theta_o}\ d(\cos\theta_o). \qquad (76)$$

Substituting Eq. (10) Eq. (76) may be solved analytically be letting $v = 3'\mu/\cos\theta_o$, so that

$$\kappa = E_1(3'\mu(E_o)) + \frac{a'}{1-b} \exp[(b-1)3'\mu(E_o)]. \qquad (77)$$

The terms in brackets in Eqs. (74) and (75) represent the true unscattered and a crude approximate total dose angular distribution respectively. To have obtained an expression for the true total dose angular distribution, the build-up factor would have to have been angularly dependent (23). The dose angular distributions become

$$\ell(d,\cos\theta_o) = (1 + a'\mu d/\cos\theta_o\ e^{\mu bd/\cos\theta_o})\ \frac{e^{-\mu d/\cos\theta_o}}{\kappa\cos\theta_o} \qquad (78)$$

and

$$\ell_u(d,\cos\theta_o) = \frac{e^{-\mu d/\cos\theta_o}}{\kappa\cos\theta_o}\ . \qquad (79)$$

The unscattered and approximate total dose angular distribution for an infinite plane isotropic source of fallout radiation were calculated for ceiling heights of 13 feet, 39 feet, 65 feet and 91 feet above the source plane. The results are shown in Figures 23 through 26. The dose angular distributions shown were calculated by superposition of thirteen dose angular distributions from plane monoenergetic source fields, in the following way:

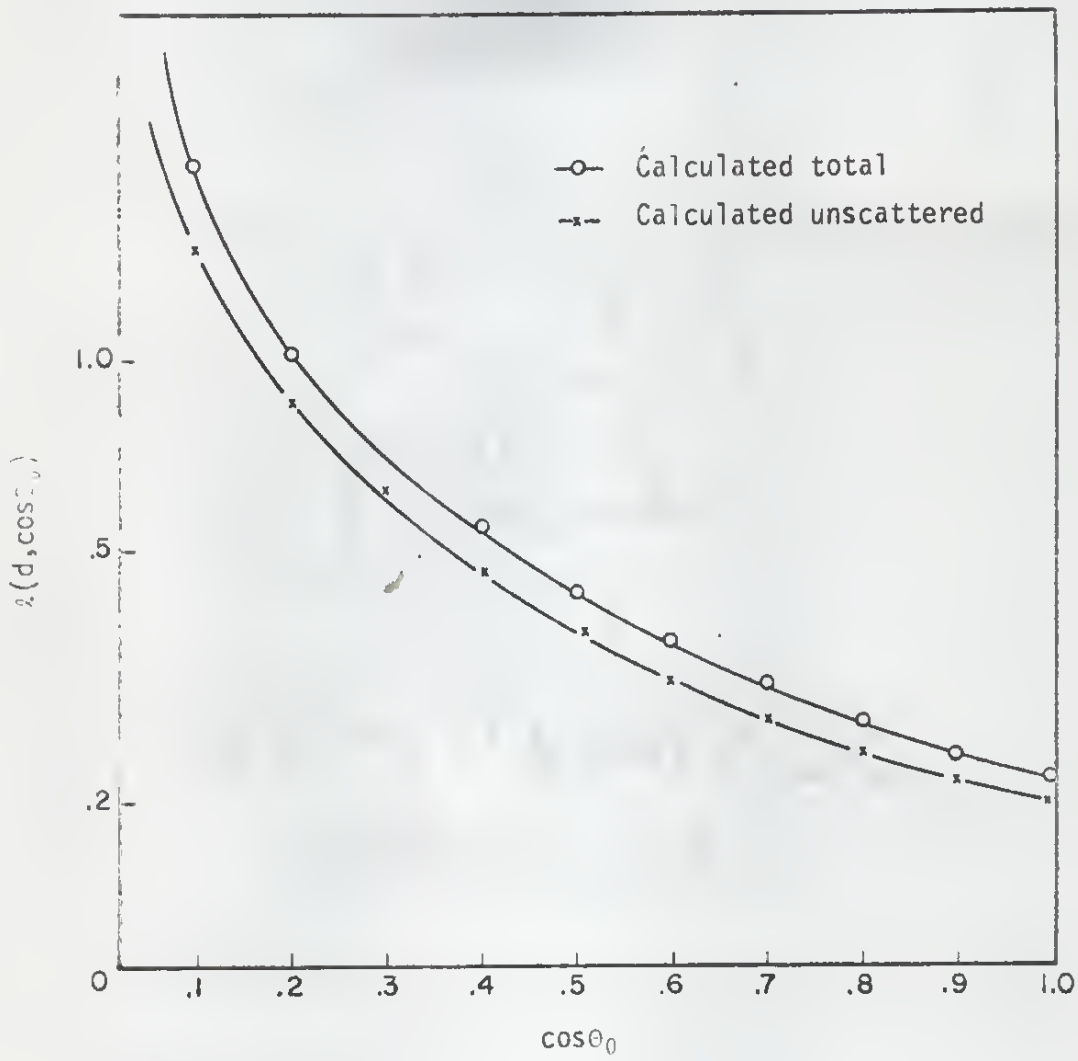

Figure 23. Dose angular distribution of radiation from a plane isotropic source of fallout radiation at 13 feet above the source plane. (U-235, 1.12 hrs.)

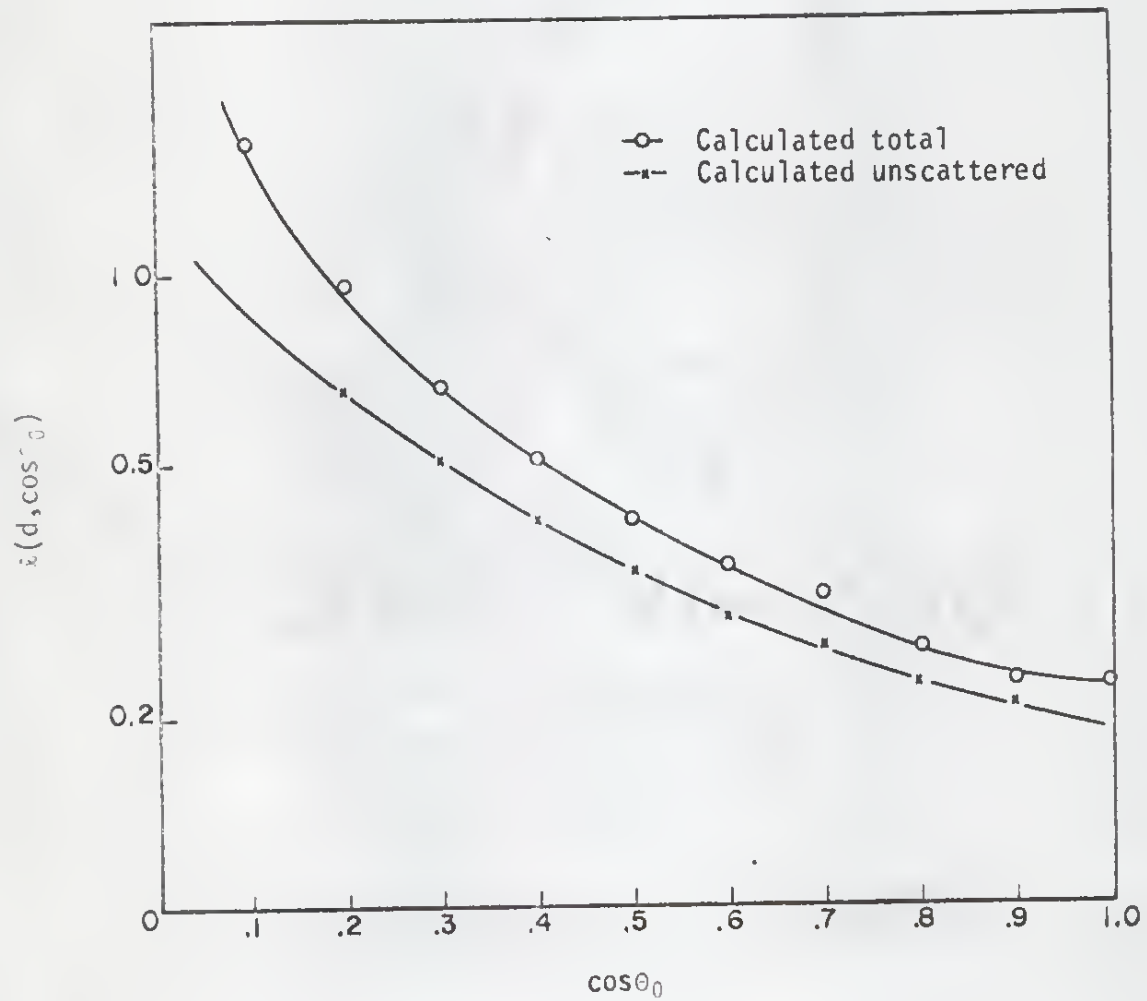

Figure 24. Dose angular distribution of radiation from a plane isotropic source of fallout radiation at 39 feet above the source plane. (U-235, 1.12 hrs.)

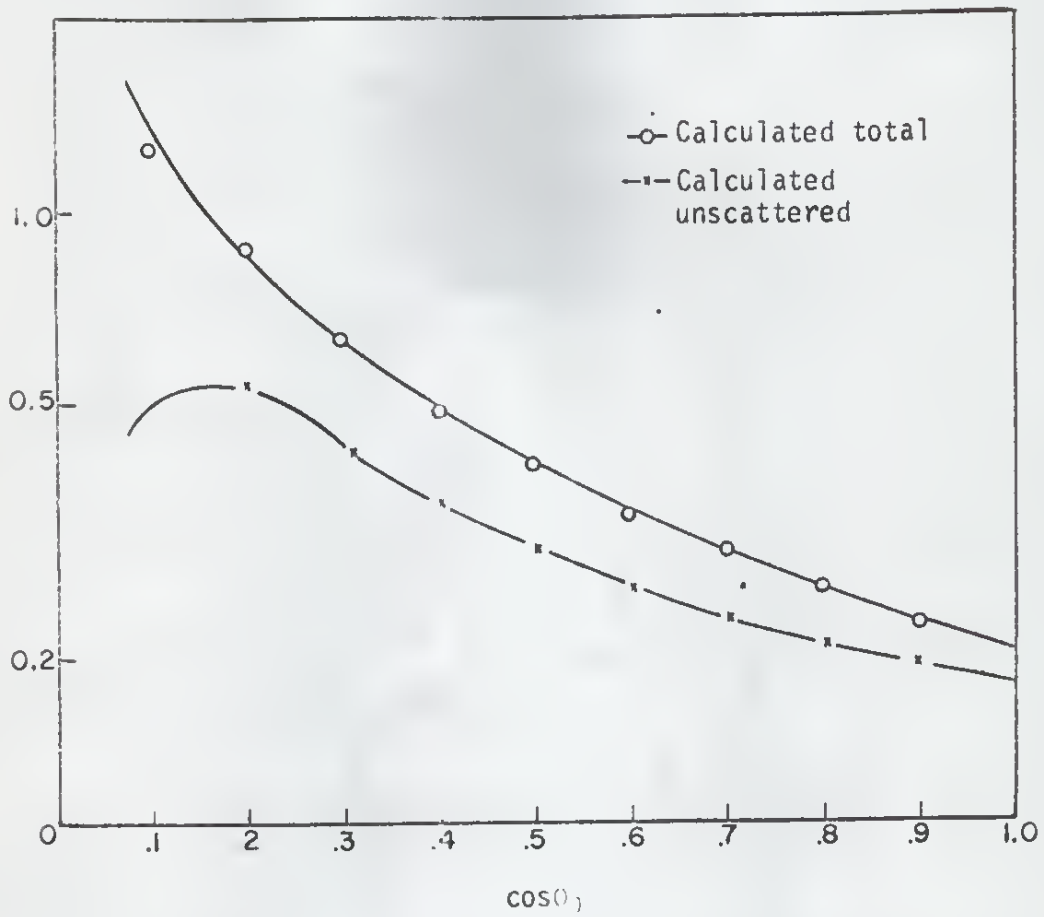

Figure 25. Dose angular distribution of radiation from a plane isotropic source of fallout radiation at 65 feet above the source plane. (U-235, 1.12 hrs.)

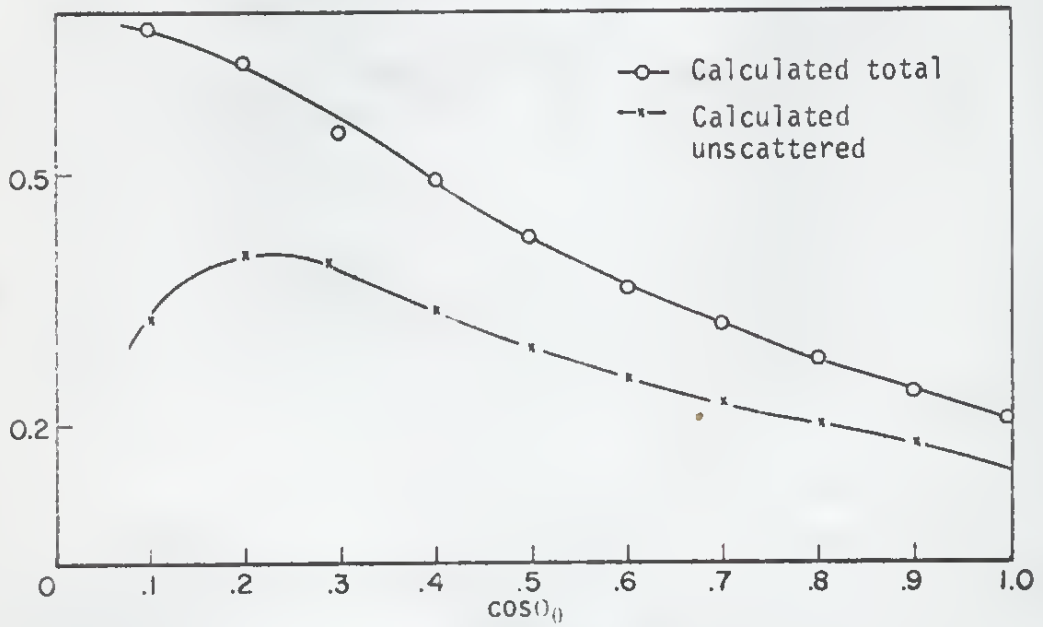

Figure 26. Dose angular distribution of radiation from a plane isotropic source of fallout radiation at 91 feet above the source plane. (U-235, 1.12 hrs.)

A. Equations (78) and (79) were solved to obtain the dose angular distribution at some height above an infinite plane isotropic field of radiation of energy equal to one of the energies of the fallout spectrum shown in Figure 1.

B. The results thus obtained were multiplied by the appropriate weighting factor corresponding to that energy contributing to the dose angular distribution of radiation from the fallout field (E_i). The weighting factors are readily obtainable from Eqs. (72) and (73) and are given by the following equation:

$$\omega_i = \frac{\mu_a(E_i)\ \varepsilon_i\ \kappa(E_i)}{\sum_i \mu_a(E_i)\ \varepsilon_i\ \kappa(E_i)} \tag{80}$$

where $\kappa(E_i)$ are given by Eq. (77), ε_i are the energy fractions of Figure 1, and $\mu_a(E_i)$ are the energy absorption attenuation coefficients.

C. An identical procedure was followed for the remaining energies of the spectrum.

D. The distributions weighted by the respective weighting factors were added to obtain the total and unscattered dose angular distribution from the infinite field of fallout radiation.

It is not meaningful to compare the calculated total dose angular distribution with that of Spencer (2). The calculated distribution is really a dose angular distribution for unscattered radiation modified in such a way that the integral of the dose angular distribution at a given height yields the dose at that height. However, the integral under the calculated distribution represents the dose at a given height and it should be equal to the dose at the

same height calculated by Spencer. To obtain the total dose rate at a given height Eq. (75) is integrated analytically. With the usual substitution, $v = \mu d/\cos\theta_0$, Eq. (75) becomes:

$$D_c = E_1(\mu d)/\kappa + \frac{a_1}{(1-b)\kappa} \exp[\mu d(b-1)]. \qquad (83)$$

The calculated dose, D_c, can then be compared with Spencer's.

Table XII. Comparison of calculated doses, D_c, to Spencer's doses, D_s, at different heights.

d (feet)	D_c	$L(d) = D_s$
13	0.73	0.76
39	0.51	0.54
65	0.41	0.44
91	0.33	0.36

It should be noted that the calculated doses did not completely agree with those of Spencer, and that the approximation for the total dose angular distribution decreases in accuracy as the distance above the source plane is increased. This can be attributed to the increase of the scattered component of the radiation as the distance above the source plane is increased. As was stated, the build-up factor used was the weakest part of the approximation. Thus, as the scattered component becomes more predominant, the error introduced by the build-up factor will increase.

The calculated dose angular distributions were used to determine the reduction factor in the center of different size structures exposed to an infinite field of fallout radiation. The form of the dose angular distribution given in Eq. (78) was used in the solution of Eq. (31).

Equation (33) was solved numerically to obtain the reduction factor in the center of different structures. The computer code, a modification of which was used for the solution, is presented and explained later in Appendix E. Table XIII lists values of the reduction factors obtained in four different square concrete structures for the thirteen energies of the 1.12 hour fission spectrum, the cobalt-60 energy and the complete fallout spectrum.

Table XIII. Reduction factors three feet above the first floor in the center of concrete structures thirteen feet high with a 5% aperture.

Source	Energy	Weight factor	Reduction Factor x 10^3			
			10'x10'	30'x30'	50'x50'	100'x100'
Fallout Spectrum	0.2128	0.01278	0.198	0.717	0.862	0.730
	0.2554	0.00286	0.186	0.683	0.835	0.733
	0.3193	0.05728	0.168	0.628	0.789	0.732
	0.4257	0.06556	0.137	0.531	0.693	0.695
	0.5108	0.01619	0.115	0.459	0.616	0.655
	0.6386	0.14252	0.090	0.368	0.518	0.598
	0.8514	0.11042	0.070	0.297	0.436	0.542
	1.0217	0.11500	0.058	0.254	0.385	0.503
	1.2772	0.10040	0.043	0.200	0.318	0.448
	1.7090	0.22088	0.027	0.140	0.238	0.367
	2.0440	0.03851	0.033	0.155	0.251	0.369
	2.5540	0.11465	0.025	0.123	0.206	0.319
	3.4060	0.00295	0.017	0.087	0.153	0.253
Total Fallout Spectrum	Fallout	1.0	0.065	0.275	0.398	0.483
Co^{60}	1.252	1.0	0.059	0.258	0.389	0.509

To compare the results obtained for an infinite source of fallout radiation with those obtained with a similar source of cobalt-60 radiation, the dose angular distribution used in the calculation of the reduction factor was normalized to a value which, upon integration, would yield the dose given by Spencer (2). It is evident that it is possible to simulate an infinite field of fallout radiation by an equivalent field of cobalt-60 radiation. Thus all calculations for reduction factors can be performed for incident cobalt-60 radiation and the results obtained are directly applicable to the actual situation of fallout radiation exposure.

The loss of accuracy involved in this approximation ranged from -10 per cent to 5 per cent. It appears to be directly proportional to the ceiling area of the structure considered. Based on these calculations, it was concluded that it was sufficiently accurate to simulate the fallout field of radiation with an infinite field of cobalt-60 radiation and thus all subsequent calculations for the design curves were performed using an infinite field of cobalt-60 radiation. For an average structure, the accuracy of simulating the fallout field of radiation by an infinite field of cobalt-60 radiation is estimated to be approximately five per cent.

APPENDIX D

Albedo Study

The total albedo is a measure of the efficiency of a surface in reflecting incident radiation. Of the three most commonly used total albedos (number, energy, and dose) only the total dose albedo will be of concern to us in this study.

The total dose albedo is defined as the ratio of the product of the number of reflected photons by their energies and by the appropriate linear (or mass) attenuation coefficients to the number of incident photons multiplied again by their energies and energy absorption coefficients. The differential dose albedo is then the fraction of photons of energy E_o, multiplied by E_o and $\mu_a(E_o)$, incident on a surface at a given θ_0 and ϕ_0, which emerge from that surface within a solid angle $d\Omega$ about Ω. The probability of that occurrence is according to reference 24, $P(E_o,\theta_0,\phi_0;E,\theta,\phi)d\Omega$.

The differential dose albedo, a_d, is therefore:

$$a_d(E_o,\Omega_0;E,\Omega)d\Omega = [\mu_a(E)E/\mu_a(E_o)E_o]P(E_o,\Omega_0;E,\Omega)d\Omega. \qquad (84)$$

The dose albedo is not the ratio of emergent dose rate to incident dose rate, since dose is proportional to energy flux. This ratio of dose rates is given by the differential dose rate albedo, $\underline{a}$.

$$\underline{a}(\Omega_0,\Omega)d\Omega = \int_0^{E_o} (\cos\theta_0/\cos\theta)a_d \, d\Omega \, dE. \qquad (85)$$

Raso (24) defines a quantity termed the "differential scattered dose rate" as:

$$SD_{jk}(E_o,\phi_0,\theta_0;E,\theta,\phi) = \int_{\phi_j}^{\phi_{j+1}}\int_{\theta_k}^{\theta_{k+1}}\int_0^{E_o} [E\mu_a(E)P(E_o,\Omega_0;E,\Omega)d\Omega\ dE] \times \left(\frac{\cos\theta_k + \cos\theta_{k+1}}{2}\right)^{-1} \tag{86}$$

These SD_{jk} represent the dose rate per incident gamma ray per cc produced by the emergent flux whose direction of flow lies within a certain solid angle, $2\Delta\Omega$.

By combining equations (84) and (86) we see that

$$SD_{jk}(E_o,\Omega_0;E,\Omega) = 2\mu_a(E_o)E_o/(\cos\theta_k + \cos\theta_{k+1}) \int_{\phi_j}^{\phi_{j+1}}\int_{\theta_k}^{\theta_{k+1}}\int_0^{E_o} a_d(E_o,\Omega_0;E,\Omega)d\Omega\ dE \tag{87}$$

and substituting this equation in (85) we obtain

$$\underline{a}(\Omega_0,\Omega)d\Omega = \frac{\cos\theta_0}{\mu_a(E_o)E_o} SD_{jk}(E_o,\Omega_0;E,\Omega)d\Omega \tag{88}$$

The differential dose rate, $\underline{a}(\Omega_0,\Omega)d\Omega$ was utilized in computing the reduction factors in structures. Because of the large number of $\underline{a}$'s required for the different incident and emergent polar and azimuthal angles, it was deemed inadvisable to attempt to interpolate among the tabulated results of reference 24. Attention was therefore devoted to semiempirical formulas which yield values for somewhat different differential dose albedos.

Chilton and Huddleston (9) developed a formula which yields values for a differential dose albedo as function of the incident and emergent polar angles and the total scattering angle between the incident and the emergent gamma ray. The theoretical derivation of this formula assumed that the

actual scattering process can be approximated by a term involving a single Compton scattering event, and another term involving isotropic scattering.

$$\alpha_d(\theta_0;\theta,\phi) = \frac{C\kappa(\theta_s) + C'}{1 + \cos\theta_0 \sec\theta} \tag{89}$$

The authors stated that the weakest part of the development was the assumption that the attenuation coefficient is not greatly dependent on energy. When, however, they compared their results with those in reference 24, they found satisfactory agreement.

The parameters C and C' were determined by a least squares analysis providing the best fit to Monte Carlo results by Raso (24), and also to similar results by Davisson and Beach (10). The parameter $\kappa(\theta_s)$ is $p \times 10^{26}$ times the Klein-Nishina cross section, where p is defined as

$$p = (E/E_o) = [1 + \frac{E_o(1 - \cos\theta_s)}{0.511}]^{-1}. \quad (E_o \text{ in Mev}) \tag{90}$$

The differential cross section per unit solid angle, Ω, derived by Klein and Nishina is given by

$$\frac{d\sigma}{d\Omega} = (R_0'p)^2[1/p + p - \sin^2\theta_s]/2 \ \frac{cm^2}{\text{elect-sterad}} \tag{91}$$

where R_0' is the classical radius of the electron,

$$R_0' = \frac{e^2}{mc^2} = 2.818 \times 10^{-13} \text{ cm.} \tag{92}$$

$\kappa(\theta_s)$ is therefore equal to

$$\kappa(\theta_s) = 3.9706 \times p^2[1 + p^2 - p(1 - \cos\theta_s)]. \tag{93}$$

Table XIV lists values of C and C' as function of incident energy. Values utilized in this thesis were obtained by interpolation among those values.

Table XIV. Parameters for semiempirical formula for differential gamma ray dose albedo (10).

E_o (Mev)	C	C'
0.2	0.0023 ± 0.0033	0.0737 ± 0.0065
0.662	0.0347 ± 0.0050	0.0197 ± 0.0035
1.00	0.0603 ± 0.0056	0.0118 ± 0.0025
2.50	0.0999 ± 0.0078	0.0051 ± 0.0011
6.13	0.1717 ± 0.0103	0.0048 ± 0.0005

The relationship between the differential dose albedo in reference 9 and the differential scattered dose rate as given by Eq. (86) is

$$\alpha_d = \frac{SD_{jk}(\cos\theta_k + \cos\theta_{k+1})/2}{1000\ E_o\ \mu_a'[2\Delta\phi(\cos\theta_k - \cos\theta_{k+1})]} \tag{94}$$

where $\Delta\phi$ is 15^o for the tabulated results of reference 21. Substituting Eq. (89) in Eq. (94), and solving for SD_{jk}, we obtain

$$SD_{jk} = \frac{1000\ \mu_a'(E_o)E_o[2\Delta\phi(\cos\theta_k - \cos\theta_{k+1})][C\kappa(\theta_s) + C']}{(1 + \cos\theta_0 \sec\theta)(\frac{\cos\theta_k + \cos\theta_{k+1}}{2})} \tag{95}$$

Again we substitute Eq. (95) in Eq. (88) and divide by $2\Delta\phi$ so as to make the resultant albedo dimensionless.

$$\underline{a}(\theta_0,\phi_0;\theta,\phi)d\Omega = 1.293[C\kappa(\theta_s) + C'][1 + \cos\theta\ \sec\theta_0]^{-1}d\Omega \tag{17}$$

The factor of 1.293 comes about from the product of 1000 times the density of air at STP. This product is necessary since μ_a' in Eq. (95) has units of cm^2/gm, and μ_a in Eq. (84) has units of cm^{-1}.

Equation (17) was used in verifying the accuracy of simulating a fallout field by an infinite plane source of cobalt-60 radiation. In calculations, however, leading to the design curves for ceiling shine radiation, using the cobalt-60 infinite field, a new and improved Chilton-Huddleston formula, utilizing seven parameters, was used. The final albedo equation, utilizing the new Chilton-Huddleston formula is (8):

$$\underline{a}(\theta_0,\theta,\phi) = 1.293\cos\theta_0 \frac{F_a(\theta_0;\theta,\phi)[C\kappa(\theta_s) + C']}{\cos\theta + \cos\theta_0\sqrt{1 + 2E_0(1 - \cos\theta_s)}} \tag{24}$$

where

$$F_a(\theta_0,\theta,\phi) = A_1 + A_2(1-\cos\theta_0)^2 + A_3(1-\cos\theta)^2 + A_4(1-\cos\theta_0)^2(1-\cos\theta)^2 + A_5(1-\cos\theta_0)(1-\cos\theta)(1-\cos\phi) \tag{25}$$

The values of the constants in Eqs. (24) and (25) are presented in Table II.

Baran (1) has compared results obtained by use of the Chilton-Huddleston formula (9) with those tabulated in reference 24. The main difference between the two appears to be at large emergent polar angles, and even so the Chilton-Huddleston formula yields a higher and therefore more conservative albedo.

Scofield and co-workers at NRDL have developed another semiempirical formula for the differential dose albedo by fitting an exponential curve to empirical data they have obtained (11). Their formula is of the form:

$$A_d(\Omega) = c' e^{-m'\theta_s} + b' \qquad (96)$$

where c', m', and b' are parameters dependent on the incident energy and the incident polar angle. The NRDL formula is probably the more accurate of the three mentioned, being derived directly from experimental data; unfortunately, however, it cannot be used in this study, since the parameters c', m', and b' are only tabulated for three distinct polar angles of incidence, and accurate interpolation to obtain the values of the parameters for the many angles of incidence required in this work, would be impossible.

The authors at NRDL have made a comparison of their results with equivalent results obtained by using the Chilton-Huddleston formula. They found that in general there was a difference of not less than 20 percent between the two values for the dose albedo, the C-H albedo being the less conservative of the two. They also stated that, although the discrepancies between the results could possibly be due to some systematic error in the Monte Carlo calculations, they felt it more likely that they be due to the use of the Klein-Nishina cross section, and that considering only incoherent scattering from free electrons was an oversimplification which was not physically accurate in the derivation of the C-H formula.

It should be said, however, that their comparison was made with the old Chilton-Huddleston formula (9), and that results obtained with the newer formula (8) might provide better agreement.

APPENDIX E

Description and Explanation of CDC-3600 Program Used to Calculate Ceiling Shine Reduction Factors

The FORTRAN source program which solves Eq. (31) is listed as Table XV. Approximately 1.5 seconds of COC-3600 computer time were required to solve Eq. (31) with a Gaussian quadrature of order three for the θ_0 and ϕ_0 integrations, order six for the y integration, and order three for the x integration (symmetry was used along the x centerline).

Total reduction factors were calculated for five ceiling areas, ten window apertures, six window sill elevations, and four ceiling heights above the source plane. The total number of points used in these calculations was approximately nine hundred.

The alphameric characters utilized in this program are defined in Table XV.

Table XV. Input data and variables required for the total reduction factor program.

Symbol	Explanation
A	Floating point constant determined by a least squares analysis, and appearing in Eq. (11).
ABSCEN	Tabulated linear absorption coefficient energies.
ACHD	Build-up parameter a' for the energy of the incident radiation.
ACHOD	Tabulated build-up parameters, a'.
ACHOOO	Build-up constant a' for reflected energy.
ANCTHE	Values for the three incident polar angles for which the average reflected energy is tabulated.

Table XV (continued)

Symbol	Explanation
ATTENU	Total attenuation of the incident radiation.
B	Floating point constant determined by a least squares analysis, and appearing in Eq. (11) as B'.
BCHD	Build-up parameter b for the energy of the incident radiation.
BCHOO	Tabulated build-up parameters, b.
BCHOOO	Build-up constant b for reflected energy.
BILDUP	Oose build-up factor for a point isotropic source (outside structure).
BUILDU	Oose build-up factor for a point isotropic source (inside structure).
C,CPRIME,CHA1 CHA2,CHA3,CHA4, CHA5	Chilton-Huddleston parameters.
CHDENG	Tabulated build-up parameter energies.
CHRTNL	Christoffel numbers in the x integration.
CHRTNO	Christoffel numbers for Gaussian Quadrature θ and ϕ integrations.
CHRTNS	Christoffel numbers in the y integration.
COMPXS	Klein-Nishina cross section times $P,\kappa(\theta_s)$.
COSTHO	Cosine of THETAO.
COSTHS	Cosine of the total scattering angle θ_s.
D	Height of ceiling above the source plane.
DESENE	Average reflected energy.
EABAIR	Total linear macroscopic gamma ray absorption coefficients for air at STP (cm^{-1}).
ENER30	Tabulated values of the average reflected energy for the 30^o incident polar angle.

Table XV (continued)

Symbol	Explanation
ENER60	Tabulated values of the average reflected energy for the 60^{0} incident polar angle.
ENER90	Tabulated values of the average reflected energy for the 90^{0} incident polar angle.
EO	Energy of incident radiation.
GAMMA	Partial contribution to the total reduction factor from the mesh points of the Gaussian Quadrature.
H	Distance from the ceiling to the window horizontal centerline (feet).
IABSC	Number of interpolation points for the determination of the total mass absorption coefficient.
IC	Fixed point x coordinate integration variable.
IJ	Fixed point θ coordinate integration variable.
IK	Fixed point ϕ coordinate integration variable.
IM	Fixed point y coordinate integration variable.
INTERP	Interpolation subroutine described in Reference 1, Appendix C.
INTRPT	Number of interpolation points for the average reflected energy determination.
KMAX	Degree of Gaussian Quadrature utilized in the θ, ϕ integrations.
LMAX	Degree of Gaussian Quadrature utilized for the x integration.
MAXENG	Number of emergent energy intervals.
MMAX	Oegree of Gaussian Quadrature utilized for the y integration.
OLEGNL	Zeroes of the legendre polynomials in the x integration.
OLEGNP	Zeroes of the legendre polynomials for use in the θ and ϕ integrations.

Table XV (continued)

Symbol	Explanation
OLEGNS	Zeroes of the legendre polynomials in the y integration.
P	Ratio of emergent to incident energies in a simple Compton scattering process.
PERCE	Percentage aperture of the window.
PHI	Azimuthal angle between positions (x,y) on the ceiling and position (xx,yy,zz) of detector, ϕ (radians).
PHIO	Arithmetic average of maximum and minimum values of the azimuthal angles subtended by the aperture (radians).
PHI1	Azimuthal limit of aperture in the positive x-plane.
PHI2	Azimuthal limit of aperture in negative x-plane.
PTHLEN	Number of mean free paths traversed by radiation from ceiling position to detector.
PTHLGT	Number of mean free paths traversed by radiation from source plane to a point (x,y) on the ceiling.
R	Half-width of the window (feet).
RHO	Distance between position (x,y) on the ceiling and position (xx,yy,zz) of the detector, ρ (feet).
SIG	Total linear gamma ray absorption coefficient (mean free paths).
SOLID	Solid angle subtended by the ceiling at the detector position.
THENER	Emergent 5^{0} polar angle intervals for the average reflected energies.
THETA	Polar angle between position (x,y) on the ceiling and position (xx,yy,zz) of detector, θ (radians).
THETAO	Arithmetic average of maximum and minimum polar angles subtended by aperture (radians).
THETA1	Polar angle subtended by bottom of aperture at given PHIO (radians).

Table XV (continued)

Symbol	Explanation
THETA2	Polar angle subtended by top of aperture at given PHIO (radians).
TOABAR	Air attenuation coefficient for the reflected energy.
TOOORA	Total reduction factor at a point (xx,yy,zz) in the structure.
V	Half-height of the window (feet).
XMAX	Dimension of the structure in the positive x direction.
XSYMTY	Has value of one when xx=0 and value of two otherwise.
XX	Oetector rectangular coordinate parallel to aperture plane, xx (feet).
XXSYM	Has value of 0 when xx=0 and value of XMAX otherwise.
YMAX	Oimension of the structure in the positive y direction.
YY	Detector rectangular coordinate perpendicular to aperture plane, yy (feet).
ZZ	Perpendicular distance measured positive downwards from ceiling to detector, zz (feet).

Logic Diagram for Ceiling Shine Reduction Factor Source Program

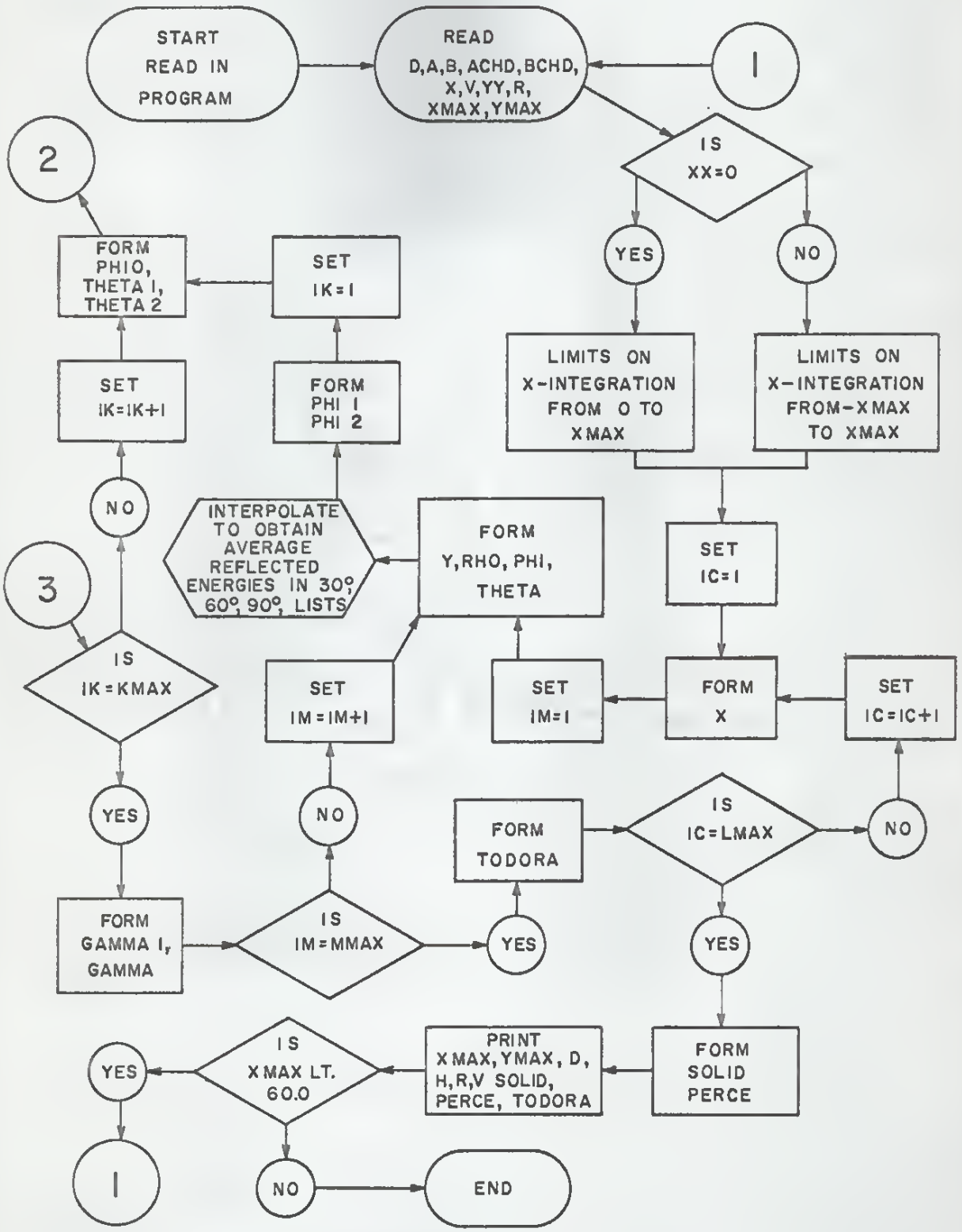

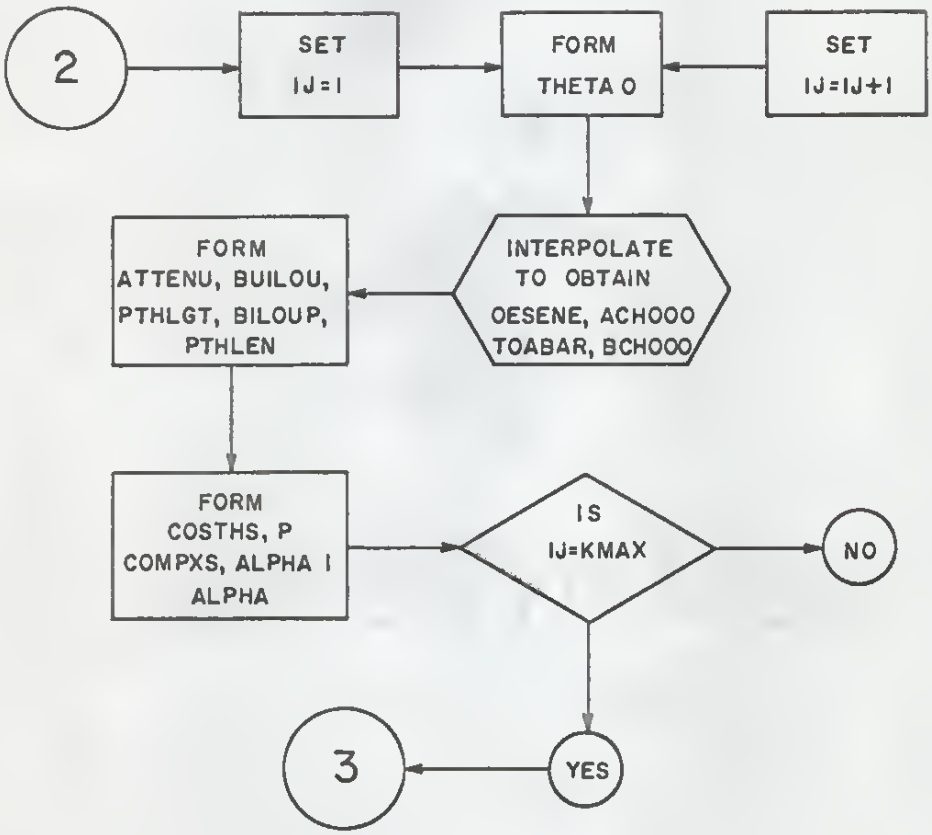
2
SET
IJ=1
FORM
THETA O
SET
IJ=IJ+1
INTERPOLATE
TO OBTAIN
OESENE, ACHOOO
TOABAR, BCHOOO
FORM
ATTENU, BUILOU,
PTHLGT, BILOUP,
PTHLEN
FORM
COSTHS, P
COMPXS, ALPHA I
ALPHA
IS
IJ=KMAX
NO
YES
3

Table XVI. Source program for the ceiling shine reduction factor.

```
      PROGRAM REDUX
      DIMENSION OLEGNP(10),CHRTNO(10),OLEGNS(20),ABSCEN(20),CHRTNS(20),
     1ENER30(20),ENER60(20),ENER90(20),THENER(20),ANCTHE(20),EN(20),
     2CHDENG(20),ACHOD(20),BCHOD(20),EABAIR(20),OLEGNL(20),CHRTNL(20)
  103 FORMAT(3X,6H XMAX=F8.4,3X,6H YMAX=F8.4,9X,3H D=F6.2)
  101 FORMAT(3X,13H SOLID ANGLE=F6.4)
    3 FORMAT(3X,3H H=F6.4,3X,3H R=F8.4,3X,3H V=F6.4)
  102 FORMAT(3X,18H PERCENT APERTURE=F6.4)
  716 FORMAT(3X,24H TOTAL REDUCTION FACTOR=F14.8,/)
  500 FORMAT(F6.2,2F10.4)
   10 FORMAT(F6.3,2F10.6)
   18 FORMAT(20I3)
   19 FORMAT(E10.3)
   20 FORMAT(7F8.4)
   21 FORMAT(F12.8)
   22 FORMAT(F11.8)
   27 FORMAT(F7.4)
  700 FORMAT(4E18.10)
      READ 18,KMAX,MAXENG,INTRPT,IABSC,LMAX,MMAX
      DO52I=1,3
   52 READ 21,ANCTHE(I)
      DO56I=1,MAXENG
   56 READ 21,THENER(I)
      DO63I=1,10
   63 READ 27,EABAIR(I)
      DO58I=1,10
   58 READ 27,ABSCEN(I)
      DO60I=1,3
   60 READ 27,CHDENG(I)
      DO61I=1,3
   61 READ 27,ACHOD(I)
      DO62I=1,3
   62 READ 27,BCHOD(I)
      DO16I=1,KMAX
      READ 22,CHRTNO(I)
   16 READ 22,OLEGNP(I)
      DO17I=1,LMAX
      READ 22,CHRTNL(I)
   17 READ 22,OLEGNL(I)
      DO655I=1,MMAX
      READ 22,CHRTNS(I)
  655 READ 22,OLEGNS(I)
   30 READ 10,EO,XX,ZZ
      READ20,C,CPRIMF,CHA1,CHA2,CHA3,CHA4,CHA5
      DO 53I=1,MAXENG
   53 READ 19,ENER30(I)
```

Table XVI (continued)

```
      DO54I=1,MAXENG
   54 READ 19,ENER60(I)
      DO55I=1,MAXENG
   55 READ 19,ENER90(I)
      READ 21,SIG
  710 READ 500,D,A,B
      READ 700,ACHD,BCHD,H,V
      READ 700,YY,R,XMAX,YMAX
   25 TODORA=0.
      XSYMTY=1.
      XXSYM=0.
      IF(XX.NE.0.0) GO TO 67
   68 XSYMTY=2.
      XXSYM=XMAX
   67 DO7IC=1,LMAX
      X=(XMAX*CLEGNL(IC)/XSYMTY)+(XXSYM/XSYMTY)
      GAMMA=0.
      DO6IM=1,MMAX
      Y=(YMAX*CLEGNS(IM)*0.5)+(YMAX*0.5)
      RHO=SQRTF(((XX-X)*(XX-X))+((YY-Y)*(YY-Y))+(ZZ*ZZ))
      IF(Y.NE.YY) GO TO 76
   77 PHI=1.5707963
      GO TO 79
   76 PHI=(ATANF((X-XX)/(Y-YY)))+3.1415927
      IF(Y.GT.YY) GO TO 79
   78 PHI=3.1415927+PHI
   79 COSPHI=COSF(PHI)
      COSTHE=ZZ/RHO
      SINTHE=SQRTF(1.-COSTHE*COSTHE)
      THETA=ATANF(SINTHE/COSTHE)
      CALL INTERP(MAXENG,THENER,ENER30,INTRPT,THETA,E30)
      EN(1)=E30*EO
      CALL INTERP(MAXENG,THENER,ENER60,INTRPT,THETA,E60)
      EN(2)=E60*EO
      CALL INTERP(MAXENG,THENER,ENER90,INTRPT,THETA,E90)
      EN(3)=E90*EO
   87 PHI1=ATANF((X-R)/Y)+3.1415927
      PHI2=ATANF((X+R)/Y)+3.1415927
      PHI1P2=PHI1+PHI2
      PHI2M1=PHI2-PHI1
      BETA=0.
      DO5IK=1,KMAX
   89 ALPHA=0.
      PHIO=(PHI2M1*CLEGNP(IK)/2.)+(PHI1P2/2.)
      COSDIF=COSF(PHIO-3.1415927)
      BILL=ABSF(COSDIF)
      THETA1=ATANF(Y/((H+V)*BILL))
      IF(H.GT.V) GO TO 90
      CTIPT2=COSF(THETA1)
      CT2MTI=-COSF(THETAI)
```

Table XVI (continued)

```
      GO TO 91
   90 THETA2=ATANF(Y/((H-V)*BILL))
      CT1PT2=COSF(THETA1)+COSF(THETA2)
      CT2MT1=COSF(THETA2)-COSF(THETA1)
   91 DO4IJ=1,KMAX
      COSTHC=((CT2MT1)*CLEGNP(IJ)/2.)+(CT1PT2*0.5)
      SINTHC=SQRTF(1.-COSTHC*COSTHC)
      THETAC=ATANF(SINTHC/COSTHC)
      CALL INTERP(3,ANCTHE,EN,2,THETAC,DESENE)
      CALL INTERP(10,ABSCEN,EABAIR,IABSC,DESENE,TCABAR)
      CALL INTERP(3,CHDENG,ACHCD,2,DESENE,ACHCDC)
      CALL INTERP(3,CHDENG,BCHCD,2,DESENE,BCHCDC)
   28 PTHLEN=TCABAR*RHC*30.48*.001293
      BUILDU=1.+ACHCDC*PTHLEN*FXPF(BCHCDC*PTHLEN)
      ATTENU=EXPF(PTHLEN)
      PTHLGT=(SIG*D*.001293*30.48)/COSTHC
      BILDUP=1.+ACHD*PTHLGT*EXPF(BCHD*PTHLGT)
      COSTHS= (SINTHC*COSF(PHI-PHI0+3.1415927)*SINTHE)-(COSTHC*COSTHE)
      P=1./(1.+(EC*(1.-COSTHS)/0.511))
      COMPXS=(3.970562)*(P*P)*(1.+(P*P)-P*(1.-(COSTHS*COSTHS)))
      DELTA=(1.-COSTHC)
      VAL=DELTA*DELTA
      VAP=(1.-COSTHE)*(1.-COSTHE)
      CHPARA=CHA1+CHA2*VAL+CHA3*VAP+CHA4*VAL*VAP+CHA5
     1*DELTA*(1.-COSTHE)*(1.-COSPHI)
      DENOM=COSTHE+(COSTHC*SQRTF(1.+2.*EC*(1.-COSTHS)))
      ALBEDC=CHPARA*((C*COMPXS+CPRIME))
      ALPHA1=(A+B*COSTHC)*ALBEDC*COSTHE*CHRTNC(IJ)*BILDUP*
     1BUILDU/(EXPF(PTHLGT)*ATTENU*DENOM)
    4 ALPHA=ALPHA+ALPHA1
    5 BETA=BETA-CT2MT1*ALPHA*CHRTNC(IK)
      GAMMA1=BETA*CHRTNS(IM)*PHI2M1*2.5723417E-2*XMAX*YMAX*CHRTNL(IC)/
     1(RHC*RHC)
    6 GAMMA=GAMMA+GAMMA1
    7 TCDCRA=TCDCRA+GAMMA
      ETA=2.*ZZ/YMAX
      GREEK=(XMAX*2.)/YMAX
      ENGLA=SQRTF(ETA**2+GREEK**2+1.)
      SOLID=(2./3.1415927)*ATANF(GREEK/(ETA*ENGLA))
      PERCE=(4.*R*V)/(26.*XMAX)
      PRINT 103,XMAX,YMAX,D
      PRINT 3,H,R,V
      PRINT 101,SOLID
      PRINT 102,PERCE
      PRINT 716,TCDCRA
      IF(XMAX.LT.60.) GO TO 710
      END
```

DESIGN OF STRUCTURES FOR PROTECTION FROM WINDOW-COLLIMATED, CEILING-SCATTERED FALLOUT RADIATION

by

ROBERTO IOTTI

B.S., Kansas State University, 1964

AN ABSTRACT OF
A MASTER'S THESIS

submitted in partial fulfillment of the
requirements for the degree

MASTER OF SCIENCE

Department of Nuclear Engineering

KANSAS STATE UNIVERSITY

Manhattan, Kansas

1967

ABSTRACT

Current engineering methods for structure shielding design and analysis do not distinguish between the separate contributions to the dose rate in a structure resulting from air scattered and ceiling scattered fallout radiation. Although the latter contribution, known as ceiling shine, is usually small, it can be a significant contribution for some situations, for instance, for buildings with a high band of windows and a roof overhang which would cut out skyshine. The purpose of this monograph is to present a method for predicting the reduction factor in multistory buildings for ceiling shine radiation.

A theoretical model is devised that yields the reduction factor in a structure due exclusively to radiation penetrating through a window and scattering off the ceiling. The final reduction factor equation, obtained from the model, is solved numerically for buildings with different floor areas, different percentage apertures in the walls, and for detectors located in different floors. Results are presented in form of charts.

Although the charts are used to determine the ceiling shine reduction factor from an infinite field of fallout, all the calculations were performed utilizing an infinite field of Cobalt-60. This resulted in a considerable reduction of the computer time needed for the solution of the problem. The accuracy of simulating the fallout field with an infinite plane isotropic source of Cobalt-60 radiation was found to be approximately five percent.

Direct use of the charts allows the determination of the reduction factor three feet above the center of any floor of a multistory regular (square or rectangular) building with floors spaced thirteen feet apart and with windows the sill height of which is not less than three feet above the floor level.

Reduction factors for oddly shaped buildings are obtained by a technique known as the "fictitious buildings" technique. Several examples accompany the graphical presentation of the results in order to aid in understanding the correct use of the charts.

No chart is presented to account for the contribution from the floor above the detector floor; this contribution, however, can be approximately obtained using existing methods. By definition there is no contribution from the floor below.

The use of the charts can be extended to buildings with floor spacing different from thirteen feet and to situations where the detector is located at a height other than three feet above the floor; this extension, however, is accompanied by a loss in accuracy.

The validity of the proposed model is also verified by comparison with existing models.